Perception and mechanical properties of the Pacinian corpuscle

A DISSERTATION
SUBMITTED TO THE FACULTY OF THE GRADUATE SCHOOL
OF THE UNIVERISTY OF MINNESOTA
BY

Tiffany Louisa (Senkow) Held

IN PARTIAL FULFILLMENT OF THE REQUIREMENTS
FOR THE DEGREE OF
DOCTOR OF PHILOSOPHY

Victor H. Barocas, Ph.D.

May 2020

Acknowledgements

I am writing this while under official "stay–at–home" orders issued by the governor of Minnesota due to COVID-19. My whole graduate school experience has been quite an adventure, and current situation will certainly be memorable. Thankfully, there have been many people who have lent me a hand throughout my time in Minnesota. I would like to take a moment to share my appreciation.

Firstly, thank you to Victor Barocas. When I first arrived in Minnesota and was meeting with students and professors, the students in the Barocas lab said that they have the best advisor; they were right. Three years ago, you reached out to me and accepted me into your lab despite my lack of background in biomechanics. I had no experience in tissue–level work, even less familiarity with neurology, and my mechanics knowledge consisted of $F{=}ma$. Even so, you took me in, and I am incredibly thankful for your mentorship, honesty, assistance, and most of all, your faith in me. Thank you for inspiring me to continue in graduate school and for working with me to create a project that is uniquely suited to my interests, abilities, and goals for my future career.

Thank you to Prof. Jonathan Sachs. Thank you for supporting me for the first few years of graduate school and during my heart surgery and the associated recovery. Thank you for ensuring my lab transfer went so smoothly and for continuing to check on me in the past few years.

Thank you to Prof. Andre Mkhoyan for including me in all your group outings and activities and for being so welcoming and approachable. Although I didn't often turn to you for science–related assistance, I appreciate your mentorship in teaching and your colorful musings on life in general.

Thank you to Dr. Amy Moeller for answering my questions about Dupuytren disease, for dissecting the hands, and for helping me test subjects at the State Fair. The projects would have turned out very differently if not for your assistance and guidance. Thank you to Prof. Raj Rajamani and Mahdi Ahmadi for designing the pressure sensor and for helping with the vibrosensitivity (aka State Fair) paper. Thank you to my other co-authors and committee members.

Thank you to all the lab-mates that I've had the pleasure of working with in the Barocas and Sachs labs. Thank you to Julia Quindlen-Hotek; your research laid the groundwork for my project and your support ensured I had a home in the Barocas lab (and especially on "Julia Island"). Thank you to Emily Chander for testing nearly all the cadaveric samples; I'm sure I would have gone mad working through them all on my own, and the results would not have been nearly as reproducible or consistent as the data collected with your hands. Thank you to the undergraduate and graduate students who have worked on the PC project

with me in the past few years. Nick, Alisha, Petra, Brianna, Sasha, and Lydia—you helped with so much behind–the–scenes work that made this project possible.

Thank you to the University of Minnesota for the facilities. I became intimately familiar with the Minnesota Supercomputing Institute using MATLAB, NAMD, VMD, COMSOL, NEURON, and other licenses. Thank you to the Driven to Discover Research Facility for helping me collect data at the Minnesota State Fair. Thank you to the countless labs that I've borrowed devices and tools from. And thank you, Kale Hedstrom and the Aerospace Engineering and Mechanics department, for "temporarily" lending me the laser velocimeter...for three years and counting.

Thank you to all the volunteers who made my thesis possible. Thank you to the Anatomy Bequest Program and especially to the donors and their families for their generous contributions. Thank you to the volunteers with Dupuytren disease who came to the University to participate in my study and to all the people who took time out of their day at the State Fair to engage in and participate in my research. And thank you to all my friends and peers who agreed to volunteer for my study when I wondered around the labs in Hasselmo Hall searching for volunteers.

Thank you to all my friends in BME and CEMS. Your support at every step along the way was critical. You immediately made me feel like part of a very diverse, encouraging, and strange family with D&D sessions and game nights, you were there to support me through academic and health turmoils, and you continue to be a great sounding board and to keep me company with texts, calls, and virtual happy hours as we're all staying at home in the interest of public health. There are a few friends who deserve a shout-out (in no particular order): thank you to Conor and Sofie for including me in several years of monthly dinners and conversations continuing well into the night, to Matt and Josh for supplying entertaining stories and endless puns and for keeping me motivated, to Ghaidan for mostly–figuratively working beside me since week one at UMN and for always being willing to help at a moment's notice, to Matt and Tyler for being trusted friends throughout college and graduate school, and to Lisa for providing a refreshing glimpse into life outside of school.

Thank you to my friends in the Minnesota Mandolin Orchestra. It was great to have a group of fun and quirky people from all walks of life and with tons of advice and experiences to share. Practices were always a wonderful escape from research stress, and the "clown car" carpool and monthly pizza nights provided great conversations about career paths and life in general.

Thank you to my friends at the Ethnic Dance Theatre. I enjoyed spending time with and performing alongside such a talented and lively group of dancers, singers, and musicians. Thank you for ensuring I had food at practice during tech-week rehearsals when I came straight from lab, for ensuring I always looked and felt my best on stage, for including me

in many intimate aspects of your lives, and for bearing with me when I was working on a tight deadline and stressed with graduate school.

Thank you to my parents. Thank you your continued support and for accepting that "my research is coming along" and for loving me enough to come to Minnesota in February! I am eternally grateful to your unconditional love.

And, finally, thank you to Jake. Thank you for always supporting me, for proofreading my papers even when it's out of your expertise area, for encouraging my teaching when I felt like the course was falling apart, for feeding me ice chips in the ICU after my open–heart surgery, for cooking me healthy meals (and occasionally brownies), and for always respecting my decisions or indecision as to my, and now officially our, future. I'm glad I get to share my quarantine with you.

Abstract

The sense of touch is processed by the somatosensory system in which mechanoreceptors are the sensory neurons that translate mechanical stimuli into neural impulses by using specialized mechanoreceptive end organs. Pacinian corpuscles (PCs), located primarily in the hairless skin of the hands and feet, are the mechanoreceptor responsible for sensing low–amplitude, high–frequency vibrations (80-1000 Hz). In this thesis, I explored how vibrotactile perception is mediated by the PCs using a combination of computational modeling, benchtop experiments on donor tissue, and psychophysical tests. There are several mechanical models of the PC, and the first part of this thesis demonstrated that a multiphysics model of a single PC contained enough details to recapitulate the trend of observed discriminability of human subjects. We showed that discriminability of sinusoidal vibrations increases as the frequency difference between the pairs increase, and we found that complex waveforms with two frequency components were more difficult to discriminate and did not follow a discernible trend. Next, we investigated the effect that Dupuytren disease (DD) has on vibrotactile perception at frequencies within the PC's range. Dupuytren disease is a progressive hand disorder in which growth and densitification of fibrous tissue in the palms eventually causes the affected fingers to bend irreversibly. DD usually presents clinically after the age of 50, affects about 3 per 10,000 adults, and is associated with alterations to the size and the internal structure of PCs. By measuring vibrotactile sensitivity in healthy and DD subjects, we found that women are more sensitive to high–frequency vibrations than men and that men with DD may exhibit reduced sensitivity compared to men without DD. We also found that, for patients in which DD presents unilaterally, the finger with DD is less sensitive than the corresponding finger on the unaffected hand. These data may serve as a useful reference to future DD researchers and may facilitate development of novel diagnostic or prognostic protocols. Finally, we designed a system to measure the viscoelastic properties of the PC and tested isolated human cadaveric PCs from donors with and without DD to better understand how the mechanoreceptor's viscoelastic properties affect vibrotactile perception.

Contents

List of Figures

Chapter 1

Introduction

1.1 Mechanoreceptors

Touch is a critical, albeit often overlooked, sense. We constantly receive tactile information about our surroundings. Right now, you can feel the force your body exerts on the chair and floor, feel the fit of your shoes, feel the fabric of your clothes, and feel which fingers are touching one another. Touch is processed by the somatosensory system, and mechanoreceptors are the sensory neurons that translate mechanical stimuli on the skin into neural impulses for our brains to decipher.

There are four primary cutaneous mechanoreceptors, each associated with an afferent neuron that uniquely responds to motion and deformation [4, 5]:

Mechanoreceptor	**Afferent neuron type**	**Sensation**
Merkel cells	Slowly adapting type I (SAI)	Pressure
Ruffini corpuscles	Slowly adapting type II (SAII)	Skin stretch
Meissner corpuscles	Rapidly adapting type I (RAI)	Light touch & Vibration
Pacinian corpuscles	Rapidly adapting type II (RAII)	Vibration

The type of afferent nerve used to deliver information to the spinal column and brain differ based on the sensation perceived of the mechanorecepto, e.g. Pacinian corpuscles are associated with slowly adaptive neurons because they require high temporal resolution, unlike Merkel cells that respond to constantly applied pressure. The specialized morphology of the end organ of the mechanoreceptor, including its associated cells and surrounding tissue, are crucial to proper function. Mechanoreceptors can function independently but often work cooperatively to deliver detailed haptic information. A schematic of mechanoreceptors in the skin is shown in Fig. 1.1.

Merkel cells respond to sustained indentation with a response that is proportional to indentation depth. They are highly sensitive to edges, points, and curves with fine spatial

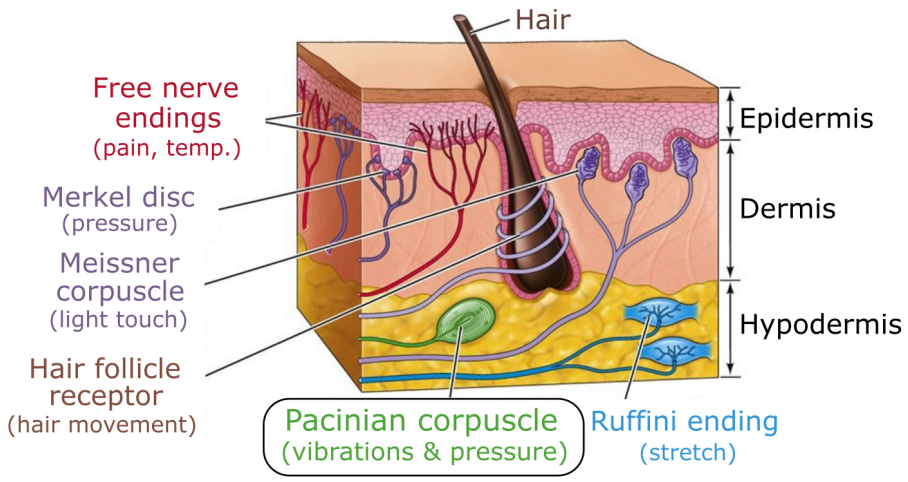

Figure 1.1: Touch receptors in skin. This diagram is only for demonstration purposes as Pacinian corpsucles and Meissner corpuscles are primarily located in glaborous (non-hairy) skin. *Figure modified from Biological Psychology textbook* [1].

resolution (0.5 mm), making them responsible for sensing an object's texture and form. Merkel cells are 10 um in diameter and located at the base of the epidermis under the sweat ducts. There are about 100 per cm^2 at the fingertip [4, 6, 5].

Ruffini corpuscles are sensitive to skin stretch, providing information on direction of object motion or force. In tandem with proprioceptors, they also sense position of the joints. They may also function as thermoreceptors. They are located in the deep dermis in both glabrous and hairy skin. Structurally, Ruffini corpuscles are elongated with tapered ends [4, 6, 5].

Meissner corpuscles are activated at the onset and offset of a stimulus but are insensitive during the static deformation. They are responsible for detecting low-frequency (5-100 Hz) vibration and slip between the skin and a held object. They have low thresholds for activation and can sense light touch but possess little spacial resolution. Structurally, they are disk-like neurite endings located close to the surface of the epidermis, between sweat ducts and adhesive ridges. Meissner corpuscles are 30–140 μm in length and 40–60 μm in diameter and densely packed (150 per cm^2) at the fingertip [4, 6, 5].

Pacinian corpuscles are responsible for sensing high-frequency (50-1000 Hz) vibrations and pressure changes. **This thesis focuses on Pacinian corpuscles, discussed in greater detail below.**

1.2 Pacinian corpuscles

1.2.1 General

Pacinian corpuscles (PCs), like Meissner corpuscles, are only activated during changes in deformation. In humans, PCs are most sensitive to vibrations around 250 Hz, which is near middle C [7, 8, 9, 4, 6]. They are responsible for sensing object fine texture and can provide dexterity for tool usage, such as controlling the tip of a pointing stick [4, 10, 11, 12]. They have low thresholds for activation (reporrted as low 10 nm deformation) [13] but large receptive fields [14, 15, 16, 5]. PCs are primarily located in the subcutaneous fat pads of glaborous skin in the hands, feet, face, and genitals, although they are also found in muscles and internal organs. Some locations with lower densities of PCs, including hairy skin like the forearm, contain single PCs whereas clusters are more common in regions of greater sensitivity [7].

1.2.2 Structure and Function

Structurally, PCs are ellipsoidal with lengths of 3-4 mm and diameters of 1-2 mm, but the shape and size varies with anatomical location and can even differ within the same cluster [17, 18]. There are 30-60 layers of concentrically-aligned lamellae surrounding a central core that contains the ending of a neurite. Inside the PC capsule, the neurite narrows and loses its myelin sheath [19, 20]. The neurite ending near the center of the PC is 8-12 μm in diameter, and there are small filopodia [21]. Near the connections to the neurite, the filopodia possess stretch-gated ion channels, which are responsible for translating the mechanical stimuli to neural impulses [19, 22, 23]. Around the neurite is the inner core of closely-packed lamellae comprised of tissue derived from Schwann cells. Growing outwards, the inner core is surrounded by the outer core, where the lamellae of epithelial-type cells spread with radially-increasing spacing [18, 7, 24, 17, 20]. The cells are flat (only 200 nm width) and bound to collagen fibrils. The lamellae are separated by viscous fluid that is prevented from entering or crossing the lamellae by tight junctions on the epithelial-like cells. Due to this structure of several layers, PCs are often referred to as "onion-like." Figures 1.2 and 1.3 show the histology and schematics of PCs.

Mechanical displacements on the skin's surface propagate to the dermis where the outer layers respond. The wave is transduced through the lamellae to the central neurite where the deformations cause the filopodia to move, thereby activating the strain-gated ion channels. The layered structure allows the PC to function as a bandpass filter; low–frequency deformations are minimized as the waveforms cannot transduce through the layers, and high–frequency components are filtered out by the limits of the neuron [25, 26, 5, 27].

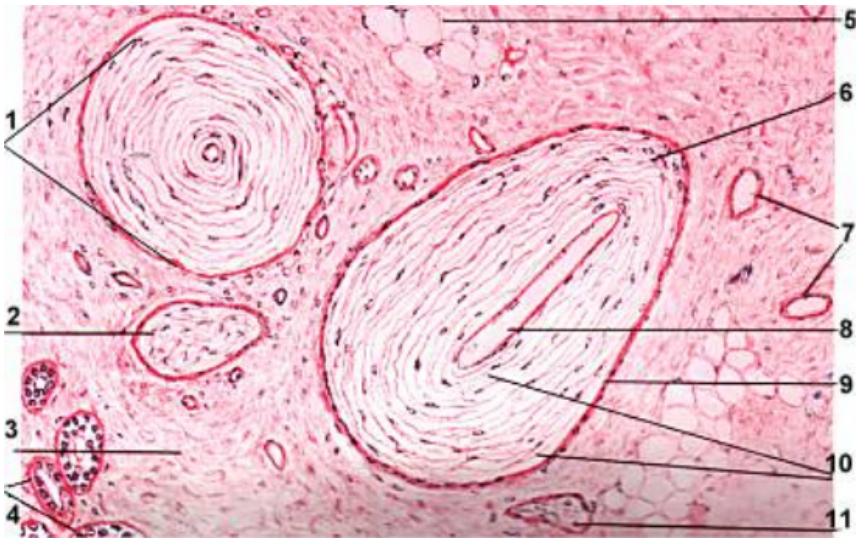

Figure 1.2: Histology of the human PC. 1. Pacinian corpuscle, 2. Nerve, 3. Connective tissue of the dermis, 4. Duct and secretory portion of sweat gland, 5. Fat cells, 6. Pacinian corpuscle: Fibroblast, 7. Venules, 8. Pacinian corpuscle: Inner core, 9. Pacinian corpuscle: Outer sheath, 10. Pacinian corpuscle: Inner and outer lamellae, 11. Nerve. *Figure from di Fiore's Atlas of Histology* [2].

1.3 Dupuytren disease

Chapters three and four of my thesis focus on Dupuytren disease and how the disease may affect the Pacinian corpuscle.

1.3.1 Clinical features and incidence

Dupuytren disease (DD) is a progressive disorder of the palmar fascia [28, 29, 30, 31], which are the fibers in the palm that anchor the skin. The disease is characterized by shortening and thickening of fibrous bands in the hands and the fingers [28]. Elevated, hard regions of fibrous tissue, called nodules, are often located in the palm; the fibrous bands may extend into the fingers, where they are called cords. Severe contracture can restrict hand function and diminish quality of life. DD is a benign fibromatosis, although the disease may be confused with soft tumors of the palm. The progression of the disease is illustrated in Fig. 1.4.

The estimated prevalence in America is approximately 7% with an annual incidence at 3 cases per 10,000 adults [32]. The disease usually presents clinically after the age of 50. The fingers most common affected are the ring and little fingers, and one or both hands can be affected without regard to handedness [29, 33]. The cause and mechanism of progression of DD are unknown, although there is a genetic disposition. It is more common in men, although the gender difference becomes less prominent with age [34]. The disease is mostly

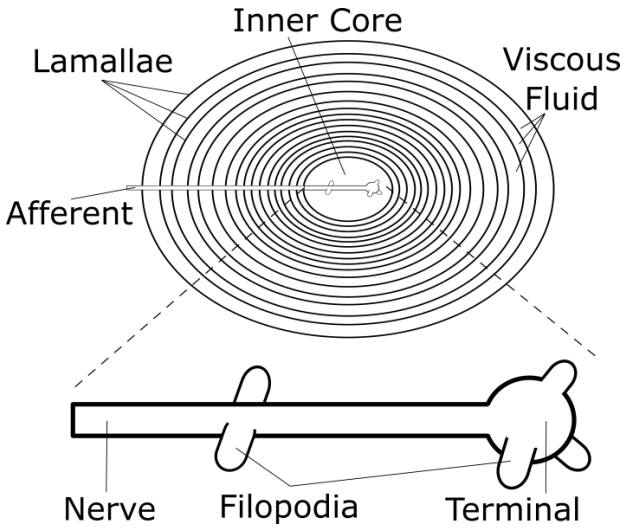

Figure 1.3: Structure of the PC. a.) Several layers of lamellae separated by viscous fluid surround an inner core and a terminal afferent nerve. The spacing between layers is exaggerated. b.) The central afferent nerve has a bulbous terminus with several filopodia with stretch-gated channels at their bases.

limited to Caucasians [35], with the majority of conditions in people of Scandinavian and British Isle descent [35]; about 20% of those over 65 in the UK have DD [29].

Histologically, the cords that characterize DD consist of a dense collagenenous matrix of fibroblasts and myofibroblasts [36, 29]. The myofibroblasts produce "large amounts of extracellular type I, III, and IV collagen depositions" [37]. The differentiation and proliferation of myofilboblasts are stimulated by various cytokines, adhesion molecules, growth factors, and and extracellular matrix compounds [37]. Many of these factors are growth– and inflammatory–related. Compared to control fascia, in tissue from DD cords, there is overexpression of genes for collagen of many types (I, III, IV, V, VI, VIII, XIV, and XV) [38]. Fibroblast proliferation and collagen deposition may create a feedback loop that progresses the disease further [35].

1.3.2 Treatment and Recurrence

DD is irreversible with no known cure. There are, however, several treatments. The gold–standard treatment for progressive DD is palmar fasciotomy. The diseased fascia is excised while minimizing removal of non–involved palmar and digital fascia [39]. A less –invasive approach is needle aponeurotomy, which uses a needle as a substitute for a blade to physically break apart the DD cords. Patients with clear cords in the palm with minimal extension into the fingers are the best candidates for needle aponeurotomy to avoid possible complications from intertwining nerves [40]. Nonsurgical intervention of collagenase enzymes were shown as safe and effective treatments to chemically disrupt the cords. Collagenase clostridium

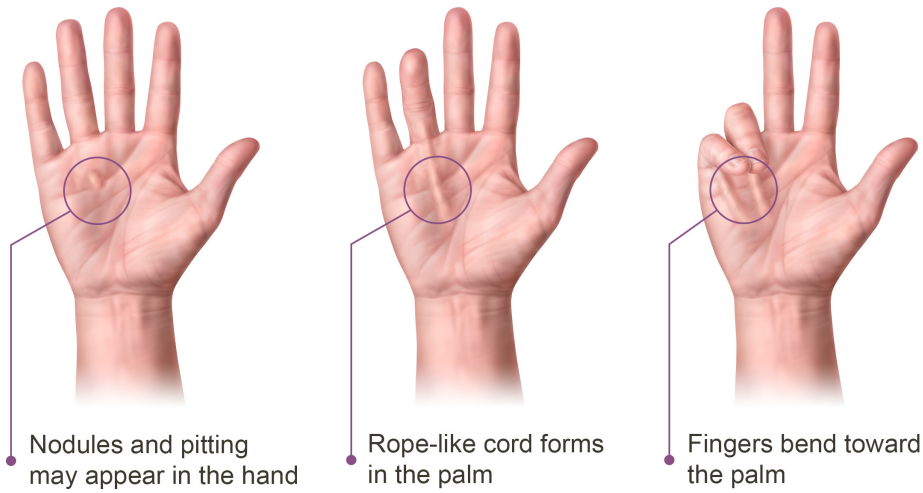

Figure 1.4: The progression of Dupuytren disease. It usually begins with nodules in the palm, followed by cords into the affected finger, and eventually contracture may occur. *Figure from Clifford Craig Foundation* [3].

histolyticum, under the name Xiaflex, was approved for use in the US in 2010 [41]. Radiotherapy was also tested on DD because proliferating fibroblasts and myofibroblasts are radiosensitive and because radiation interferes with growth factors and inflammatory cytokines. Radiotherapy may slow disease progression at early stages when surgery is not an option [42], and research of its use is ongoing. There are other non–surgical treatments that are ineffective or deemed unsafe for clinical use [41]. Some unsuccessful treatments include include ultrasonic therapy, dimethyl sulfoxide (DMSO) injections, topical vitamin A and E, physical therapy, corticosteroid injections, 5-fluorouracil treatment, and gamma interferon injections [41].

Relapse after surgical excision is common. There are six factors that affect aggressiveness of DD and likelihood of recurrence after treatment:

1. Ethnicity
2. Family history of one or more affected siblings or parents
3. Bilateral DD
4. Ectopic lesions in the knuckle (Garrod pads)
5. Male gender
6. Age of onset younger than 50 years

It is estimated that there is a baseline risk of recurrence after surgery of 23% for patients

who have *none* of the above factors; the risk of recurrence increases to 71% for those with *all* the above factors [43].

There are three extrapalmar lesions that are similar to DD and often occur in patients with DD [44].

- *Ledderhose disease*: Fibrosis of the plantar fascia in the foot
- *Peyronie disease*: Fibrosis of the penile shaft causing anterior angulation
- *Garrod pads*: Fibrotic lesions of the dorsal digital fascia of the proximal interphalangeal joint in the knuckles

1.3.3 Relationship with Pacinian corpuscles

There have been several studies that reported structural changes in the PCs near Dupuytren nodules and cords [18, 45, 46, 47, 48, 49]. These changes to PCs in Dupuytren–related tissue compared to healthy patients include

- increased size [47, 46, 45, 49, 50, 51],
- more numerous lamellae [47], and
- more collagen [50].

Based on these changes, we predicted that patients with DD may have different sensitivities to vibration and that the viscoelastic properties of the PCs from Dupuytren–related tissue would also differ from healthy PCs. **The relationship between PCs and DD was studied in chapters 3 and 4**.

1.4 Summary of internal chapters

The key research studies of my thesis are organized in the following three chapters. Each chapter is summarized below.

Chapter 2: Computational and psychophysical experiments of the Pacinian corpuscle's ability to discriminate complex stimuli [52]. This study concentrated on how well the PC can differentiate stimuli of different frequencies. We compared a multiphysics model of a single PC with psychophysical experiments on healthy volunteers. We measured discriminability of two stimuli in two categories: simple and complex stimuli (i.e. chord waveforms with a higher frequency and an underlying 100 Hz frequency component). To test subjects, we created a device using a piezoelectric buzzer inside a clip that volunteers wore on the index finger of their dominant hand, and subjects subjects felt two vibrations separated by a brief pause

then answered whether the stimuli were the same or different. Discriminability of the simple stimuli increased as the frequency difference between the paired stimuli increased. Complex stimuli were more difficult to discriminate in both the model and the psychophysical studies and did not follow any discernible trend. From this experiment, we demonstrated that the multiphysics model of a single PC contains enough details to recapitulate the trend of the observed response of human subjects when discriminating vibrations. This study was published in *IEEE Transactions on Haptics* [52].

Chapter 3: Vibrotactile perception in Dupuytren disease. This study investigated the ability to sense vibrations with and without DD. Based on the enlarged size of PCs in DD subjects, we expected that subjects with DD would present altered sensitivity to high-frequency vibrations and that the changes would be most prominent around 250 Hz, where healthy subjects are the most sensitive. We designed a device to deliver vibrations of specific frequencies and amplitudes to the fingertip and palm. The minimal thresholds of sensitivity were determined with in 36 subjects with DD and in 74 subjects without DD. We found that sensitivity decreases with age, which agrees with findings by others. Women showed greater sensitivity than men and men exhibited lower sensitivity in DD vs. healthy subjects, but the latter results were not statistically significant. In subjects with DD presenting unilaterally, the unaffected hand was more sensitive than the affected hand. These data on vibration sensitivity present interesting trends that may serve as a useful reference to future DD researchers.

Chapter 4: Viscoelastic parameters of the Pacinian corpuscle. This study concentrated on the viscoelastic properties of the PC. Although mechanical models of the PC exist, the viscoelastic properties, chiefly the Young's modulus and the viscosity, are estimates. We created a cantilever–based device and a corresponding COMSOL model to determine the viscoelastic properties of PCs at physiologically–relevant timescales, i.e. 50-500 Hz range. Based on the additional collagen and more lamellae in PCs from subjects with DD, we expected a change in the size and the mechanical properties of the PCs from the DD patient compared to the PCs from non–DD donors. The PCs from a human cadaveric donor with DD were significantly larger than the PCs from two donors without DD, although it would not be appropriate to draw conclusions about changes in DD based on only on three donors. Preliminary values of a Young's modulus of 86 Pa and a viscosity of 0.86 Pa·s were determined from a representative PC, and recommendations to improve the ongoing optimization were discussed.

Chapter 2

Computational and Psychophysical Experiments on the Pacinian Corpuscle's Ability to Discriminate Complex Stimuli

The content of this chapter has been published as a research article in *IEEE Transactions on Haptics* by Tiffany L. Senkow, Nicholas D. Theis, Juliam C. Quindlen-Hotek, and Victor H. Barocas [52].

2.1 Summary

This paper assesses whether the difference between responses of two stimuli predicted by a multiphysics model of the Pacinian corpuscle correlated with the observed psychophysical discrimination between them. The simulation's response, estimated by the van Rossum distance, was compared to psychophysical same–different experiments and studied with simple sinusoidal stimuli and complex stimuli, i.e. waveforms with an underlying 100 Hz frequency component. Estimated discriminability of the *in silico* experiments correlated well with the psychophysical experiments, suggesting the multiphysics model of a single receptor can be used to study PC behavior. Discriminability of the simple stimuli increased as the frequency difference between the paired stimuli increased; complex stimuli were more difficult to discriminate in both the model and in the psychophysical studies and did not follow any discernible trend.

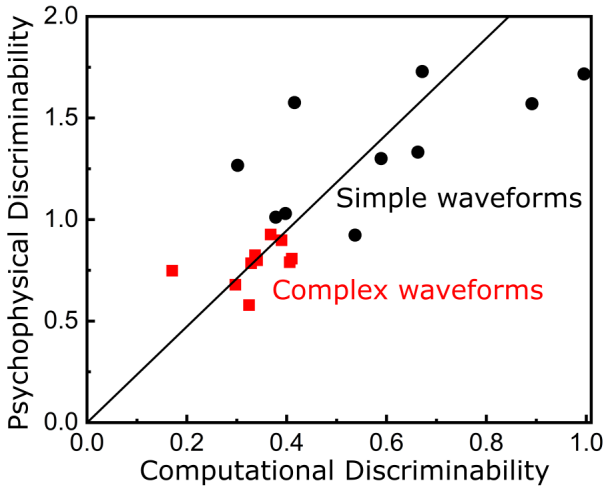

Figure 2.1: The subjects' ability to distinguish between the simple stimuli increased as the frequency increased, a result consistent with the model predictions for the same stimuli. The model also predicted correctly that subjects would find the complex stimuli more difficult to distinguish than the simple ones and also that the discriminability of the complex stimuli would show no trend with frequency difference.

2.2 Introduction

The Pacinian corpuscle (PC) is a dermal touch receptor responsible for transducing high–frequency vibrations, making it a central biological component for haptic processing. PC afferents primarily innervate the palm and fingers, but they can be found in other areas of the body as well [53]. PCs have limited spatial resolution but are highly sensitive to skin deformations, with amplitude sensitivity on the order of 10 nm [4, 13]. The PC, along with related touch receptors, has seen a recent resurgence of interest driven in part by the pursuit of better haptic technology and by efforts towards developing somatosensory prosthetics [54, 55, 56, 57]. A deeper understanding of PC physiology also offers potential biomedical applications of haptic technology.

In the adult human hand, each PC afferent neurite ends in a single ellipsoidal corpuscle, with an average length of 1 mm and average width of 0.7 mm [23]. The outer core of the corpuscle consists of several lamellar layers (approximately 30 in healthy adults) of collagen–associated epithelial–like cells separated by fluid [17]. The structure has been the subject of numerous modeling efforts [58, 59, 60, 61, 62, 63] since the seminal work of Loewenstein and Skalak [27]. In the computational models cited above, the PC is modeled as shells interspersed with thin layers of fluid. These fluid–spaced lamellae in concert with the rapidly adaptive type II neuron act as a bandpass filter [25], removing low–frequency vibrations that are sensed by other mechanoreceptors [26, 5].

The mechanistic models described above face a fundamental challenge in terms of valida-

tion because of the ethical and practical challenges associated with performing a physically invasive experiment on humans or non–human primates. Isolated PCs can be studied mechanically [27, 64, 18] or functionally [8, 65], but the experiment is difficult, especially for the latter case, and isolated tissue studies are difficult to relate directly to somatosensation. Thus, although the mechanistic models can provide broad understanding, their applicability has been limited. A new approach is clearly needed, for which we can look to strategies used in the analysis of simpler models.

Previous studies of the neural representation of touch stimuli have relied on behavioral experiments combined with electrophysiological recordings [8, 65, 66, 67, 68, 69]. Some work examined the PC's ability to encode more complex vibrations, in particular polyharmonic stimuli [66, 70, 71, 30], and made efforts to draw inferences about the neural code [72, 73, 11, 74]. Horch [66] studied discrimination of high-frequency complex stimuli, investigating the effects of phase shift, concluding that discrimination of complex stimuli was dependent neither on frequency nor on amplitude but on the peak acceleration. Conversely, the Bensmaia group conducted similar studies and found that PC afferents convey frequency information of frequency and timing [11] and that pairs of the same frequencies at different phases were hardly distinguishable from each other [72]; this observation led them to contend that discriminability was influenced by power. In a follow-up study using both psychophysical and *in silico* experiments [74], it was concluded that individual spectral components were conveyed through what the authors termed "quasi–independent mini–channels," suggesting that polyharmonic stimuli are distinguishable at the population level even if they may not be distinguishable by a single PC, an idea that could also be explored in more depth using the population models recently presented by Saal et al. [63].

Following this general experimental paradigm, it may be possible to combine psychophysical data with simulated spike trains to evaluate the simulation's relevance and to explore neural encoding computationally in lieu of invasive experiments. Thus, the goal of the present study was to assess this approach by comparing relevant psychophysical measures of various stimuli with model predictions of the response to the same stimuli. Employing this combined psychophysical–experimental approach, we explored the extent to which stimuli perceived as different by experimental subjects were also measurably different in terms of the output generated by a previously–published multiphysics model of the PC response [62]. The current work narrows the conditions of frequency discrimination and operates under the assumption that van Rossum distance is an adequate measure of difference between simulation outputs [75]. We performed parallel psychophysical experiments on human subjects and *in silico* experiments with the computational model using two sets of stimuli: 1) a single, pure sinusoidal waveform, which can be compared with previously reported studies, and 2) a waveform consisting of the same sinusoidal component and

an underlying 100 Hz sinusoidal component, which investigates discrimination with more complex stimuli.

2.3 Methods

2.3.1 Frequency Selection

For both the *in silico* and the psychophysical experiments, stimuli were drawn from two stimulus sets: simple and complex. Simple stimuli consisted of single–frequency pure sinusoidal waves within the 100-500 Hz range. Complex stimuli were formed by adding an equal–amplitude 100 Hz component to each waveform from the simple set. Henceforth, we name a stimulus by its frequency, followed by an "S" for simple stimuli and a "C" for complex stimuli. For example, 160C refers to a complex stimulus formed by combining a 100 Hz wave with a 160 Hz wave (both sinusoidal), and 160S refers to a pure 160 Hz sinusoid. The frequencies selected for this study were 160, 230, 310, 400, and 500 Hz (Fig. 2.2); these stimuli were assumed to excite mostly PCs because they all lie within the reported PC sensitivity range (40-800 Hz) and largely out of the reported most sensitive range of Meissner corpuscle afferents (10-100 Hz) [5]. The difference between adjacent pairs of selected frequencies increases linearly between 70 Hz and 100 Hz. Discriminabilities between pairs were only assessed within sets; discrimination was not att empted between simpler stimuli and their complex counterparts.

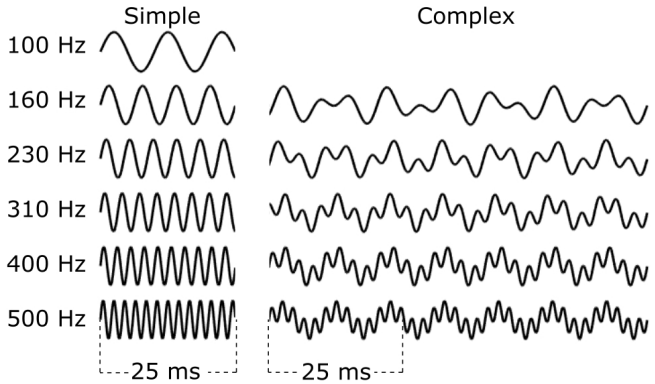

Figure 2.2: Stimuli used in psychophysical and *in silico* experiments. The 10 stimuli tested, from two stimulus sets, are shown. The simple, sinusoidal waveforms (S) are shown on the left, and the corresponding complex waveforms (C) are on the right. The stimuli are shown on the same scale, however, the amplitude for the higher frequencies was slightly lower than that of the lower frequencies.

Previous psychophysical experiments with 100 Hz - 300 Hz stimuli reported that the just-noticeable difference (JND) follows Weber's contrast, $\Delta F/F_{lower}$, with an average constant

across frequencies of approximately 0.2 [74, 76, 77, 78], whereas one study found the Weber fraction for the JND to increase with frequency [79]. Because the frequency pairs selected for this study have $\Delta F/F_{lower}$ values greater than the previously reported difference limens, we expected all of the simple stimuli pairs to be discriminable and thus to constitute a good basis for comparison with the discriminabilities of the complex stimuli.

Notably, complex waveforms of two components undergo phases of constructive and destructive interference, resulting in an enveloped waveform where the frequency of constructive phases, that is the beat frequency, is equal to the magnitude of the difference between the two components [80]. An earlier study on consonance and dissonance perception of vibrotactile chords [71] concluded that the dominant sensory cue for dissonance is beat frequency (i.e. the smallest envelope between the two frequency components), regardless of the base frequency used. In this study, the stimuli had beat frequencies of 60 Hz, 130 Hz, 210 Hz, 300 Hz, and 400 Hz (Fig. 2.2). Selecting different beat frequencies ensured there would be no bias toward similar pairs. We chose to select some but not all frequencies that were divisible by the base frequency, 100 Hz, as that may influence discriminability.

2.3.2 Psychophysical Same–Different Experiments

Forty-three adult subjects (ages 18 - 44) participated in psychophysical testing; some participated up to three times on different experimental days. There were a total of 74 individual tests. Experiments were IRB–approved and carried out under IRB guidelines by a CITI–trained investigator. Subjects were seated and placed the tip of their dominant index finger on a pirzoelectric disc bender (APC International, Ltd. 20-1330) in a clip applying light pressure. Vibrotactile stimuli were delivered to the subjects by a piezo wired directly a digital–to–analog signal generator (Syscomp WGM-201, Ontario) that was controlled via MATLAB. Analog signals to the actuator were amplified (Gemini XGA-3000, New Jersey) to 30 V, the maximum input voltage of the vibrating piezo, and were not altered ebtween expermients or subjects. The piezos were characterized under no load with a vibrometer controller and fiber interferometer (Polytec, OFV-2600/OFV-352); we measured the correcponding acceleration between 100 Hz and 500 Hz to be 130 dB - 150 dB (ref. $10^{-6} m/s^2$), which is greater than the vibrotactile perception thresholds for healthy persons.

A same–different test [81] was used to determine whether the subjects could significantly discriminate between the stimuli. Subjects were presented with two 1.5-second stimuli from the same stimulus set (simple or complex) separated by a 0.5 second pause. The stimuli were either the same or different, and the order in which pairs were presented was randomized. After being presented with a stimulus pair, the subjects were prompted by the computer to answer whether the stimuli were the same or different. The subjects had

at least two practice trials in which they were told that the stimuli were different; they could repeat the practice trials as many times as desired. Subjects were not instructed to base their decision on frequency or amplitude differences. During all testing procedures, subjects wore headphones playing gentle rain sounds to mask the sound of the piezo and other ambient sound that might distract them or provide unintended auditory cues. Each separate stimulus set (simple or complex) consisted of 40 trials. For each subject, each same pair was repeated 4 times and each different pair was repeated twice, maintaining a 50:50 balance of same and different stimuli. The subjects had the opportunity to rest for as long as needed after every 20 trials — most subjects paused for 10 to 20 seconds. The duration of the entire experiment, including consent and a brief explanation of the subject's results, was an average of 25-30 minutes. To improve subject alertness and to test a wide range of frequencies, we concentrated only on the frequency discrimination and not amplitude effects. The results were summarized by 10 discriminability values per stimulus set.

The discriminability measurement, d', was determined using the same–different differencing rule, which is preferred when multiple comparisons are made during the same experiment [81, 82, 83] and does not make assumptions about the direction of difference or the attribute responsible for the difference [84]. The probability of a correct response is determined from the hit rate and false alarm rate for a given stimulus pair. The hit rate is the probability that the subject responds "different" when the two stimuli are different, and the false alarm rate is the probability that the subject responds "different" when stimuli are the same. Rates from individual subjects were calculated separately because participants may belong to different populations. For an overall perspective, the data were averaged to calculate a single d' value for each paired stimuli. The d' value for each comparison was determined by referring to the tables in the appendix of [81]. The bias parameter, k, was calculated from the normal distribution and the false alarm rate [81]:

$$k = -\sqrt{2}\Phi^{-1}(A/2) \tag{2.1}$$

where Φ^{-1} is the inverse normal cumulative distribution function and A is the false alarm rate.

2.3.3 Simulated Discriminability Measurements

The PC was simulated using a three–stage model as previously described [58]. In the first stage, the fluid-spaced lamellae of the outer core are modeled as spherical shells. Simulated mechanical stimuli were applied to the outermost lamella (shell) and propagated to deeper shells through the fluid–filled spaces between lamellae using equations from shell theory and lubrication theory. In the second stage, the deflection of the inner–most shell from the first

stage was applied to the inner core of the PC, modeled in COMSOL as an incompressible solid sphere surrounding an isotropic, linearly elastic neurite with realistic geometry, including filopodia extruding from the neurite surface, which are hypothesized to be the sites of mechanically–gated ion channels [23, 19, 61, 7].

In the third stage, membrane currents were calculated based on strains at the base of each of the five filopodia using a sigmoidal function of the directional strains as previously described [10]. Strain waves were rectified by zeroing negative values under the assumption that stretch–gated channels are opened by positive strains but remain closed under zero or negative strains. Current injections were scaled with the minimal linear amplifier required to produce a spiking rate equal to the stimulus frequency, i.e. to reach the tuning threshold, for all simple frequencies. Scaling allowed for the modeled stimuli, like the stimuli in the psychophysical setting, to be delivered at an intensity relative to a measurable threshold. Stage–three simulations were run in NEURON with Hodgkin–Huxley channels [85]. Action potentials from the resulting voltage traces were defined as peaks occurring above an action potential threshold value, which was varied between -60 mV and 0 mV in 1 mV intervals. Each simulation ran for 1 second of stimulated stimulus, and the entire duration was analyzed.

The neurite membrane strains for complex stimuli were calculated directly by summing results of the filopodial strains generated by the constituent single–frequency waves from stage 2 of the model. This algebraic addition was possible because the first two model stages are linear. For the third, electrophysical, stage of the model, the summed, complex strains were converted to current injections and used to calculate voltage traces.

Spike trains were compared using the van Rossum distance (VRD) [75]. Discrete spike trains X and Y were transformed into continuous functions by convolving each spike with an exponential

$$x(t) = \sum_{i}^{n} \mathrm{H}(t - t_i) exp[-\frac{t - t_i}{t_c}] \tag{2.2}$$

where $\mathrm{t_c}$ is a time constant, $\mathrm{t_i}$ is the time of spike i, n is the length of the signal, and H is the Heaviside step function. The resulting signals, x and y, were then used to calculate the van Rossum distance

$$VRD(x, y)_{t_c} = 1/t_c \int_0^\infty [x(t) - y(t)]^2 dt \tag{2.3}$$

The resulting VRD were normalized with a maximum of 1. After an initial analysis of $VRDs$ using t_c values between 25 µs and 2.5 ms, we chose to use a t_c of 500 µs, which was the most consistent with the psychophysical results and lies within estimates of the high temporal precision of PCs [11].

2.4 Results

2.4.1 Psychophysical Results

The mean discriminability values calculated for simple and complex stimuli comparisons exhibit two salient features. The overall trends are most evident when the individual subjects' d' values are averaged, as shown in Fig. 2.3a and 2.3b. Firstly, the simple stimuli are easier to distinguish than their complex counterparts. Secondly, the simple stimuli appear to follow a trend where the discriminability, represented by the mean d' values, increases as the frequency difference, or ΔF, increases. For example, the 160/400S and 160/500S pairs, which have large ΔFs, have mean d' values of 1.7 whereas the 310/400S and 400/500S pairs have mean d' values of only 0.9 and 1.0, respectively. However, the complex stimuli do not appear to follow any trends.

With a limited number of trials of each comparison, there are only seven possible d' values for each subject. The distribution of both the simple and complex pairs, as well as the *d'* values for each subject, are provided in the Appendix the end of this chapter. A d' value of zero indicates an inability to discriminate the pair (i.e. no improvement over random guess) and is caused by the subject responding correctly for fewer than four of the six stimuli. The complex comparisons contain a greater proportion of zero d' values than the corresponding simple pairs, indicating that the complex stimuli were more difficult to discriminate. Following the trends of the averaged data, the simple stimuli pairs that have frequencies with a greater ΔF contain a lower proportion of zeros, again suggesting greater discriminability on an individual level. The individual data were plotted with $\Delta F/F_{lower}$ and fit using a linear regression that was free to have a nonzero intercept. The stimuli with a greater $\Delta F/F_{lower}$ were more discriminable for the simple stimuli (mean slope = 0.44, p = 0.0004), as shown in Fig. 2.3c, but that effect was less pronounced for the complex stimuli, shown in Fig. 2.3d, where the mean slope did not significantly differ from zero (mean slope = 0.06, p = 0.261). A negative slope for the best fit of the $\Delta F/F_{lower}$ vs. d' indicates that the individual subject more accurately discriminated between pairs with lower ΔF than pairs with higher ΔF — this effect may reflect an overall lack of discriminability or may be due to the small number of trials.

In general, the mean hit rates were similar for both simple and complex stimuli (0.58 and 0.56). However, the false alarm rate increased for the complex data (from a mean of 0.4 for simple stimuli to 0.5 for complex stimuli), causing the bias parameter, k, to differ from mean values of 1.34 for the simple stimuli to 1.02 for the complex stimuli. In other words, subjects appeared to require weaker evidence for the complex signals before responding that the signals were different.

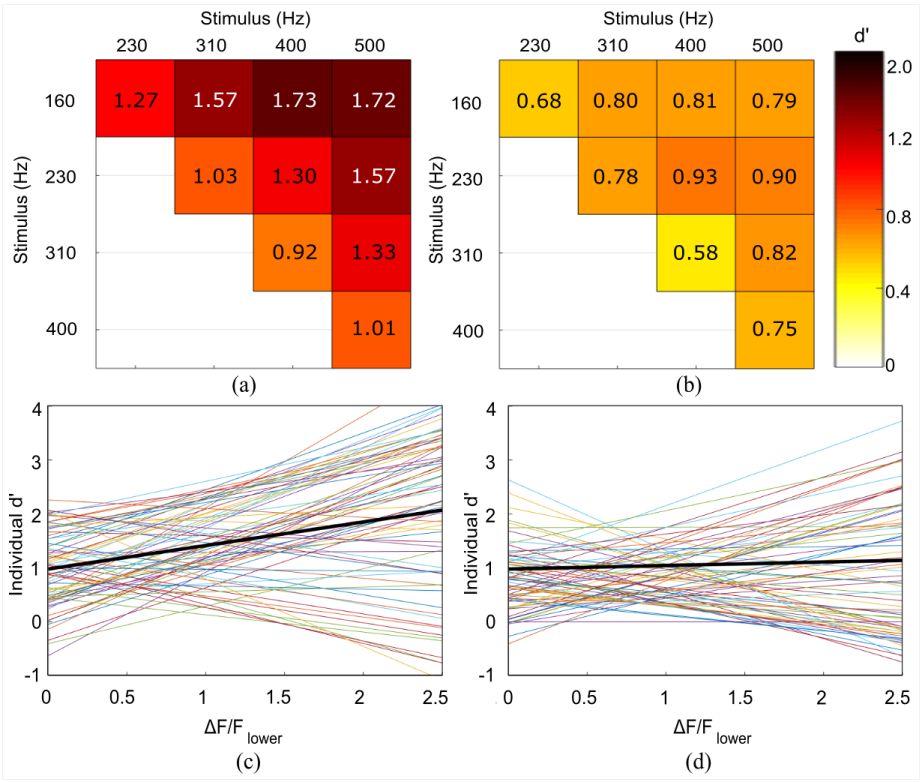

Figure 2.3: Psychophysical Experiment Results. (a,b) Discriminability (d') for each frequency comparison in the (a) simple (single frequency) and (b) complex (with 100 Hz base frequency) cases. The colorbar shows the relevant d' values for both cases. (c,d) Discriminability of (c) simple and (d) complex stimuli pairs as a function of $\Delta F/F_{lower}$ fraction. The colored lines show the linear fits for individual subjects; the thicker black line the average linear fit.

2.4.2 *In Silico* Experiments

PC activity was simulated for the ten stimuli (five simple and five complex) examined in the psychophysical setting. For simple stimuli, the normalized current traces of any individual filopodium synchronized to the stimulus pattern, possibly with a phase shift. The lower frequencies, however, experienced much greater strain amplification during stage 1 and 2 and, therefore, larger currents and final voltages, as shown in the black waveforms in Fig. 2.4a. When the strains were summed *in silico* to create the complex waveforms, the amplitude of the two components, although of equivalent intensity on the corpuscle surface, differed by as much as a factor of nine at the filopodia surface due to frequency–dependent transmission through the lamellae. Upon conversion from strain to current with the sigmoidal function, the peaks that experienced destructive interference were drastically attenuated or eliminated. The voltage traces shown in red in Fig. 2.4a illustrate that the interference followed through phase 3 of the model.

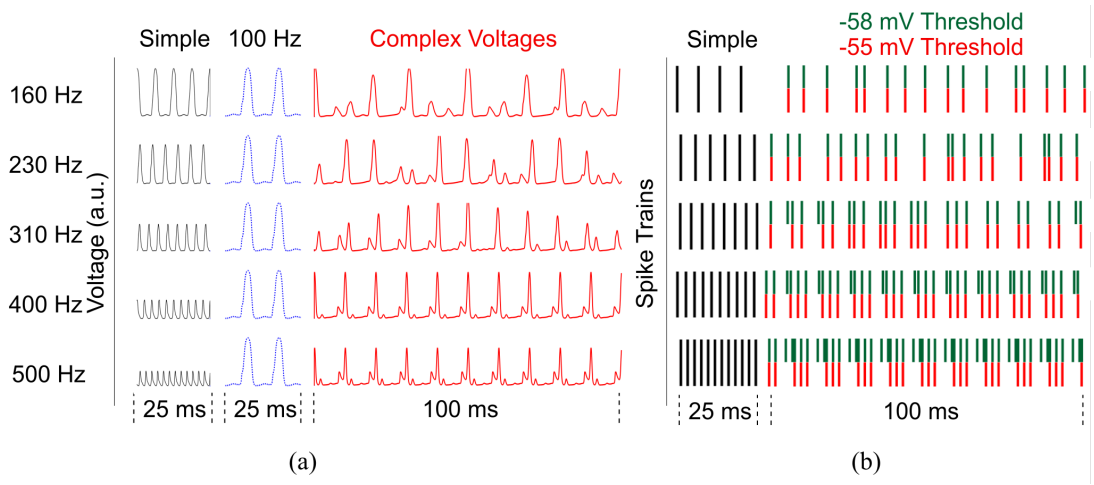

Figure 2.4: *In Silico* Experiment Results.(a) Normalized voltage traces of phase 3 output. Simple waveforms (red lines), the 100 Hz waveform (dotted blue lines), and the complex waveform (solid black lines) are shown on the same scale for each frequency. The lower frequency, simple voltage traces have greater amplitudes due to strain amplification; because of this effect, the 100 Hz component of the complex waveform is more prominent than the higher frequency component and some interference patterns, such as those on 100/310C, are visible. (b) The neural spike trains of the simple waveform with the -55 mV action potential threshold (other action potential thresholds gave similar results) (black lines) and the complex waveform with from the -55 mV action potential threshold (green, top half) and from the -58 mV action potential threshold (red, bottom half). The same range is shown for both voltage and spike trains.

The *VRDs* calculated for comparisons involving only simple waveforms followed the same trend as the psychophysical results and were independent of the threshold potential, that is the depolarization voltage at which the neuron initiates an action potential, within the tested range. The *VRD*s for the complex waveforms, however, showed action potential–dependent response. We anticipated that the PC stimulated with complex stimuli would phase–lock with either the higher frequency or the beat frequency. Instead, the nerve with complex stimuli fired at rates between those of the simple low and high frequency components due to regions of destructive interference (Fig. 2.4b). Specifically, if the action potential threshold was set at or below -58 mV (i.e. 7 mV above the resting potential), the spike trains, especially those with higher frequency components, were distinct from each other (Fig. 2.4b) and the model results for the complex waveforms (Fig. 2.5b) were very similar to those for the simple waveforms. In contrast, for higher thresholds (e.g. -55 mV, Fig. 2.5c), the spike trains were more alike (Fig. 2.4b), and the predicted differences in *VRD*s were well below those for simple stimuli. Furthermore, the *VRD*s for the complex waveform pars were smaller than those for the corresponding simple waveform pairs (Fig. 2.5d), a result consistent with the psychophysical observations. If was also found that the

higher (-55 mV) threshold led to less $\Delta F/F_{lower}$ sensitivity (Fig. 2.5c), again consistent with the psychophysical results. Based on these observations, we concluded that the -55 mV action potential threshold was the appropriate choice, and we used only that value in subsequent analysis.

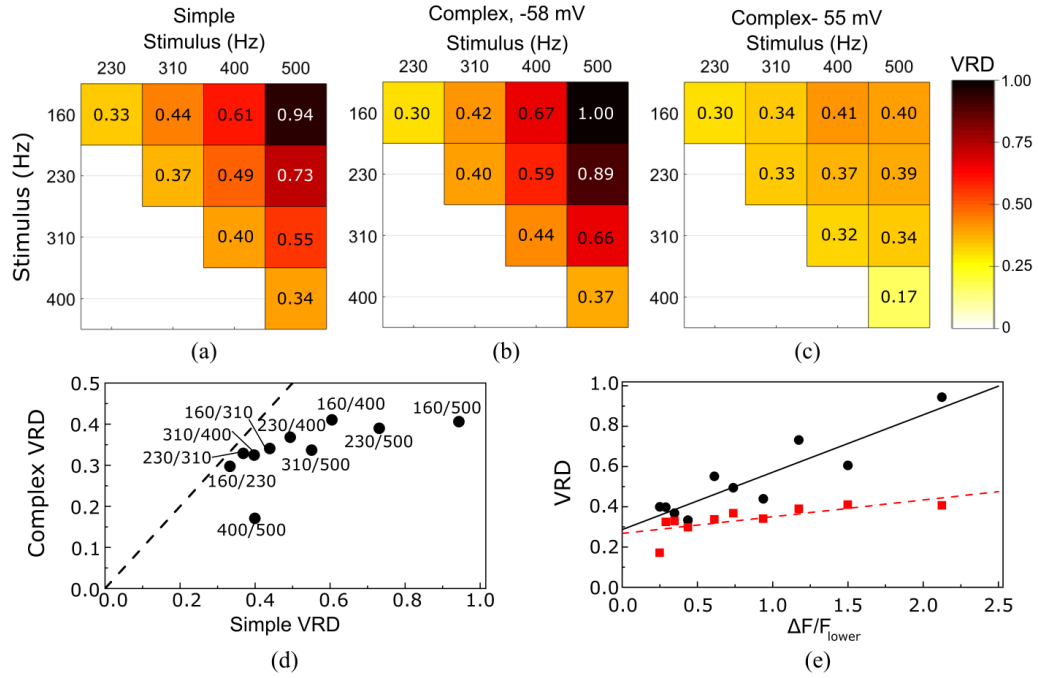

Figure 2.5: *In Silico* Experiment Results. (a-c) van Rossum distance (*VRD*) for each frequency comparison for (a) simple stimuli at an action potential of -55 mV (other action potential thresholds gave similar results), (b) for complex stimuli at an action potential of -58 mV, and (c) for complex stimuli at an action potential of -55 mV. The colorbar shows the relevant *VRD* values for all cases. (d) Discriminability of simple vs. complex stimuli for each pair. Pairs are labeled on the plot. The dotted line is $y{=}x$; points below this line are more discriminable in the simple case. (e) Discriminability of simple (black circle) and complex (red square) pairs with the action potential of -55 mV as a function of $\Delta F/F_{lower}$ ratios. The black line shows the linear fit of the simple data; the red line the linear fit of the complex data.

2.4.3 Comparison of Psychophysical and Simulation Experiments

For a given stimulus pair, it is possible to plot the psychophysical discriminability value, *d'*, against the *in silico VRD* value for the same pair. A plot of this type, shown in Fig. 2.6, reveals that the discriminability calculations for the psychophysical and *in silico* experiments for the simple stimuli are correlated with each other, as shown with the fitted line. Conversely, both the *d'* and *VRD* values for the complex data with the -55 mV threshold are clustered together with neither the psychophysical nor the *in silico* experimental data

following a clear trend apart from having lower values than their simple counterparts. A linear fit of both the simple and complex data sets ($d' = VRD/0.42$, $R_{adj}^2 = 0.247$, $p =$ 3e-14) shows general consistency between the *in silico* and psychophysical results.

2.5 Discussion

2.5.1 Psychophysical Experiments

The primary purpose of this study was to evaluate the simulation's ability to predict *in vivo* discrimination of stimuli; to assess the model, we compared *in silico* results to psychophysical experiments. Additionally, we wanted to confirm the psychophysical trends, especially those with complex stimuli, with existing findings. To compare with previous literature, we estimated discriminability with d' values.

The psychophysical experiments suggest that discriminability of simple vibrating stimuli in the range of PC activation (100-500 Hz) increases as the frequency differences between the paired stimuli increase, which agrees with multiple previous studies [66, 70, 71, 72, 73, 74]. Since the majority of the frequency differences in the current study were near or above the reported JND, the observed high discriminabilities for simple stimuli were expected and were consistent with but not as large as those reported by Bensmaia et al. for a similar simple–stimulus study [74]. The largest difference between the two studies studies is that we had far more individual subjects with fewer trials for each stimuli comparison while Bensmaia et al. [74] had fewer subjects with multiple trials. Other differences in *d'* values could be due to other factors such the training regimen, the frequencies tested, or the vibrator used to deliver the stimulus, all of which varied slightly between the studies.

Complex stimuli with an underlying 100 Hz waveform were more difficult to discriminate than their simple counterparts and did not follow any discernible trend in discrimination. Many of the individual *d'* values for the complex stimuli were zero, which caused the mean *d'* values to be lower than those for the simple stimuli. A *d'* of zero was caused by subjects responding incorrectly in at least half the trials, which by itself illustrates poor discriminability. Several linear regressions of *d'* vs. $\Delta F/F_{lower}$ calculated negative slopes for the complex stimuli, further indicating poor discriminability. While the specific complex frequency components differed from previous studies [72], both studies found a lack of discrimination for the complex pairs. This could be explained by nonlinear mechanical amplifications through the skin or the PC, by the nerve being unable to reliably encode both components, or by the somatosensory system being unable to recognize the neural signals as different.

Stimuli were delivered at intensities several times larger than the detection threshold

for the lower frequencies tested but closer to the detection thresholds of some subjects for the higher frequencies. It is, therefore, possible that responses may have been influenced by changes in perceived intensity. Some previous studies [74, 86, 87, 88, 89, 90] reported that perceived intensity may influence frequency discrimination, whereas others [66, 72, 91, 92] concluded that frequency discrimination is not significantly affected by changes in amplitude, provided the stimulus intensities are significantly higher than the perception amplitude. Additionally, the clip on the fingertip may have applied more pressure to some subjects than to others, which may have added variability.

An explanation for the greater bias in the simple vs. complex studies is not evident. The subjects performed both the simple and complex studies during the same sitting, received the same instructions and training, were exposed to no external changes in stimulus presentation, had no feedback until both experiments were completed, and faced no consequences for their responses.

2.5.2 Simulation Experiments

The model was evaluated in its ability to replicate the psychophysical trends, but some additional parameters outside the initial model were needed for analysis, especially for the complex data; these parameters include the time constant in the *VRD* calculation and the action potential threshold. We will discuss the effects of these parameters.

First, the van Rossum distance provided an estimate of the difference between the *in silico* voltage outputs. For the simple stimuli, the *VRD* was consistent with a rate code or interspike interval because the stimuli are synced at the start of the simulation, that is they can be referenced to the same absolute starting point. The analyzed t_c values were selected such that the higher–frequency stimuli did not produce significantly larger *VRDs* compared to the lower–frequency stimuli merely due to the higher–frequency stimuli creating more voltage spikes. The final selection of 500 µs is on the same order of magnitude as that found previously [11].

Second, the selection of action potential threshold was critical. If a threshold value were too close to the resting potential, then small increases in the voltage would trigger spurious action potentials in the simulation. Small–amplitude artifacts interpreted as action potentials could result in greater apparent differences between the frequencies, i.e. greater discriminabilities, up to a point at which the artifacts would drown out the signal and make all frequencies indiscriminable. Conversely, if an action potential threshold value were too high, then the voltage would never exceed the threshold, and no action potentials would be registered, also presenting all frequencies as indiscriminable. Whereas the exact threshold for human PCs is unknown, thresholds of rapidly adapting neurons from spider

mechanoreceptors have been measured at -41.6 ± 13.9 mV (26.5 above resting potential) [64] and -53.6 ± 6.91 mV (8.53 mV above resting potential) [93, 94]. Additionally, investigations in threshold voltages found that the occurrence of previous action potentials can influence neuron excitability [95]. In this study, there were large differences between the complex waveforms for thresholds at -58 and -55 mV (7 and 10 mV above the resting potential, respectively) (Fig. 2.4b and Fig. 2.5b,c). Considering that both action potential thresholds appear to be reasonable estimates, and accepting that the selected Pacinian corpuscle and neuron model parameters surely introduced error, we cannot exclude the possibility of either result. However, the slightly higher thresholds produced *VRDs* in better agreement with the psychophysical discriminabilities. For the complex stimuli, there were sudden changes in the *VRD* values as the action potential threshold was further raised (e.g. at -35 mV, data not shown) — these correspond to the smaller peaks in the interference pattern not registering as nerve spikes. The simulated response to simple stimuli was not affected by the selection of action threshold potential in the range analyzed.

Earlier studies have suggested that the PC has a strong tendency to phase–lock its spike rate with simple stimulus frequencies at supra–threshold levels, suggesting a rate code in which the firing rate of the nerve indicates the stimulus frequency [4, 61, 8, 65, 68]. Other studies, primarily focusing on other mechanoreceptors, have concluded that stimulus in formation is derived from the mean interspike interval of afferent cells [8, 96, 97, 98], a finding that is not at odds with the rate code hypothesis. Rather than rely on the rate code or interspike interval as outputs, we used *VRD* as an estimate of discrimination. However, *VRD*s still consider individual spikes, and the spike trains were dependent on the action potential threshold, as shown in Fig. 2.4b.

2.5.3 Comparison of Psychophysical and Simulation Experiments

In this study, we explored the ability of the single afferent model to recapitulate psychophysical results with both simple and, as a more demanding challenge, complex stimuli. For a given stimulus pair, it is possible to plot the psychophysical discriminability value, *d'*, against the *in silico VRD* value for the same pair. A plot of this type, shown in Fig. 2.6, reveals that the discriminability calculations for the psychophysical and *in silico* experiments with the -55 mV action potential threshold correlated well with each other. Although there are some nonlinearities where the *d'* is different from the expected discriminability from the van Rossum distance that reduce the goodness of fit, the trend between the *in silico* and psychophysical experiments is clear in Fig. 2.6. The inverse slope of the line, 0.42, may be compared to the standard deviation of the signal value in the classical derivation of *d'*. That is, if one imagines that the responses to two stimuli can be plotted on some linear

scale and have means separated by the van Rossum distance when so plotted, then one can postulate an apparent signal standard deviation, σ_{VRD} of 0.42, making

$$d' = \frac{VRD}{\sigma_{VRD}} \tag{2.4}$$

in the imagined space. Such a space does not actually exist, and this construct has no physical meaning per se, but rather serves as a useful conceptual tool when comparing the *in silico* and *in vivo* results.

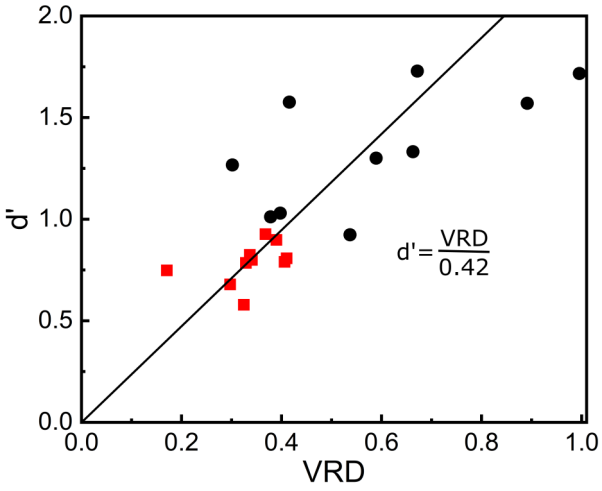

Figure 2.6: Comparison of Psychophysical and *In Silico* Experiment Results. The x-axis denotes the van Rossum distance from the *in silico* experiments with the action potential thresholds of -55 mV; the y-axis corresponds to the *d'* measured in the psychophysical experiments. Discriminability of simple stimuli (black circles) and complex stimuli (red squares) shown as the mean of the individual *d'* values. The black solid line denotes the linear relationship for the simple waveforms forced through the origin ($d' = VRD/0.42$, $R_{adj}{}^2 = 0.247$, $p = 0.3\text{e-}14$).

To realize that promise, numerous challenges and shortcomings with the current study would need to be overcome. Perhaps most important is that in the finger, multiple PCs would be engaged, particularly considering our fairly large (10 mm diameter) vibrator, whereas the model simulated a single PC. Also, all the experiments were done at the same amplitude, which meant that at high frequencies, the amplitude may not have been far above the detection threshold for some subjects, which could introduce considerable error in limiting analysis to frequency discrimination. Furthermore, the simulations were all noise–free, whereas some imperfections must have occurred in the psychophysical processing of the vibratory information. The van Rossum distance, moreover, serves as an estimate of synchrony between afferent spike trains, and, although it correlated well with

the psychophysical discriminability, *VRD* does not directly measure discriminability.

These results can be considered in light of Bensmaia's contention that the more complex the signal, the more important the population encoding becomes [72]. In the current study, a single PC afferent, not a population, was modeled. Although there is a large population of PCs with large receptive range in the fingertip [53], our *in silico* simulation of a single PC correlated with the psychophysical response, suggesting that a single PC could encode sufficient information to distinguish signals of the type studied. It is likely that, although the complex stimuli in the current study were more sophisticated than pure tones, they were still straightforward enough to be identified by a single detector, but more complex waveforms, e.g. stimuli with more than two components or harmonics, may require population coding, perhaps via the 'mini-channels' suggested by Bensmaia et al., through cooperation of PCs tuned to different frequencies, or by involvement of other mechanoreceptors. It is also likely that although a single-PC model can predict trends in discriminability, the population of PCs in the hand provides much higher sensitivity levels than a single PC could. Finally, although stimulus location was not examined in the current work, a population code may play an important role in localization, as suggested by theoretical studies [99].

2.6 Conclusion

Discriminability as predicted by *VRD*s in the *in silico* experiments correlated well with the discriminability observed in the psychophysical experiments, demonstrating that a multi-physics model of a single receptor can be used in conjunction with psychophysical experiments to study the behavior of the PC. These psychophysical experiments suggest that discriminability of simple (i.e. pure sinusoid) vibrating stimuli in the range of PC activation (100-500 Hz) increases as the frequency differences between the paired stimuli increase, agreeing with previous studies [66, 70, 71, 30, 72, 73, 74]. Complex stimuli with an underlying 100 Hz waveform were more difficult to discriminate and did not follow any discernible trend, also similar to reported findings [74]. The discriminability of simulated spike trains, estimated by the van Rossum distance, for the complex stimuli was dependent on the time constant and the action potential threshold, but agreed with the psychophysical results when appropriate parameter values were used. We calculated the σ_{VRD}, the *VRD* value where one would expect the *in silico* model to be discriminable. Further, we note that, although we used a model developed by our group, other mechanical models of PC function [59, 60, 63, 27] could also be used; we would expect them to require different tuning but to demonstrate similar predictive capacity.

Further investigations should explore alternative encoding/discrimination schemes as well as the possibility of a population code. This study of PC encoding raises more ad-

vanced questions of PC population behavior, e.g. how PC activity is integrated to produce meaningful sensations, which our single–PC model is unable to address. Understanding somatosensation poses a greater challenge still, as touch information is encoded by multiple specialized afferents and is processed centrally. In principle, all of these components could be modeled. The tuning of such a multiscale model and the re–tuning for changes due to, e.g. aging or disease, will surely require a validation approach beyond threshold or discriminability measurements. What the current study suggests, however, is that the multiphysics model is also a behavioral model. That is, a single PC modeled in sufficient detail is able to recapitulate some of the observed response of the whole organism to a simple behavioral assay. This ability may provide opportunities to evaluate the structural changes or variation in PC physiology, as well as a more systematic investigation of the PC's role in the neural representation of more haptic sensations across populations of receptors.

2.7 Appendix: Distribution of *d'* values for each frequency comparison

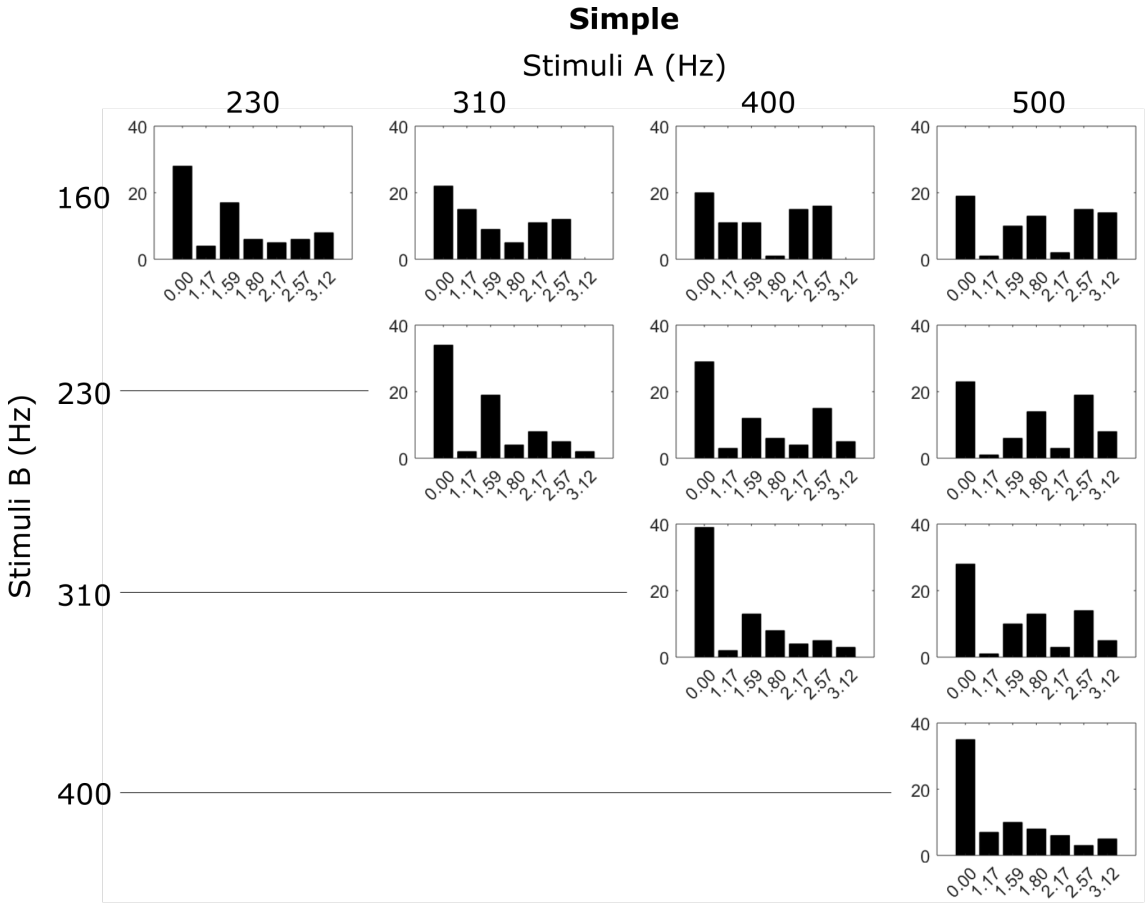

Figure 2.7: Psychophysical experiment results. Distribution of *d'* values for each frequency comparison for simple stimuli is shown.

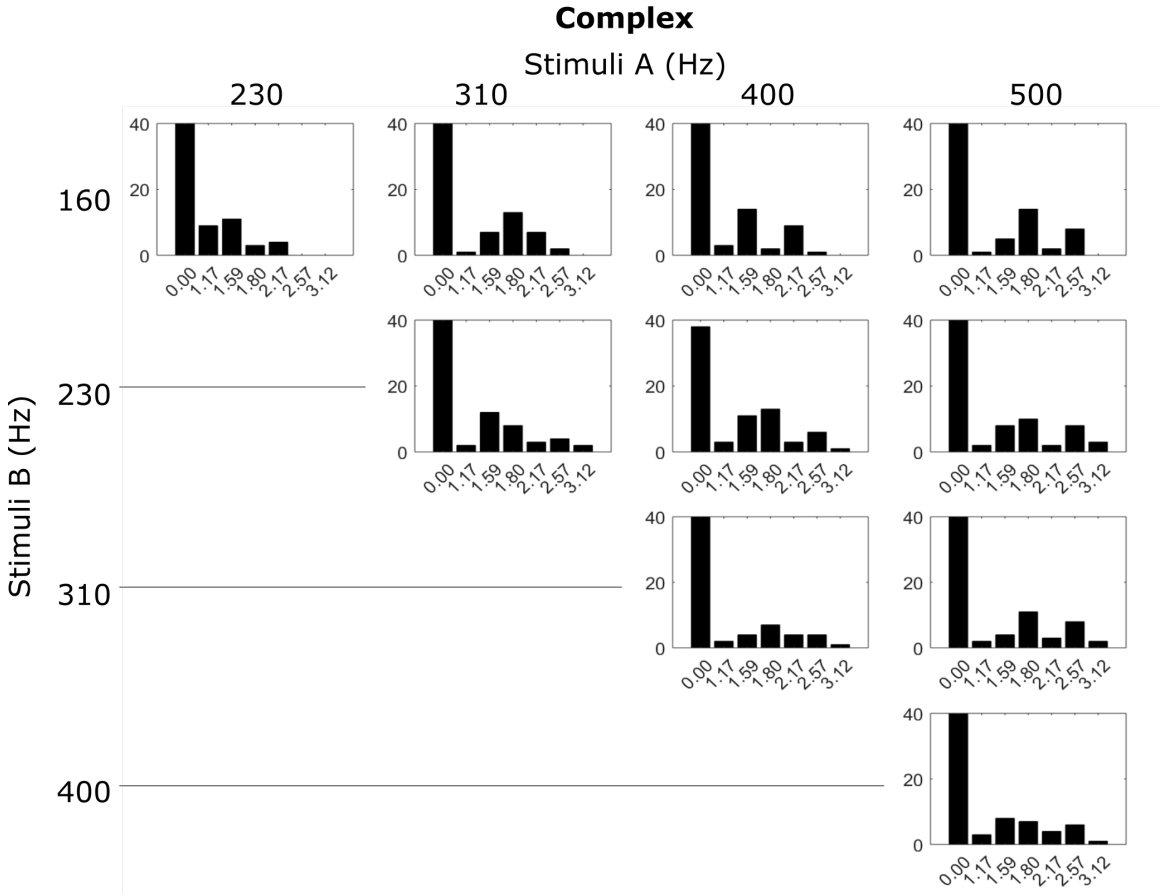

Figure 2.8: Psychophysical experiment results. Distribution of *d'* values for each frequency comparison for complex stimuli is shown.

Chapter 3

Vibrotactile perception in Dupuytren disease

The content of this chapter has been submitted as a research article to the *Journal of Plastic Surgery and Hand Surgery* by Tiffany L. Senkow, Mahdi Ahmadi, Rajesh Rajamani, Victor H. Barocas, and Amy T. Moeller and is under review [100]. The dataset is available on Mendeley [101].

3.1 Summary

Dupuytren disease (DD) has been associated with enlarged Pacinian corpuscles (PCs) and with PCs having a greater number of lamellae. Based on these associations, we hypothesized that subjects with DD would have altered sensitivity to high–frequency vibrations and that the changes would be more prominent at 250 Hz, where healthy subjects demonstrate the highest sensitivity. A novel device was created to deliver vibrations of specific frequencies and amplitudes to the fingers and palm. Using a Psi–marginal adaptive algorithm, vibrotactile perception thresholds (VPT) were determined in 36 subjects with DD and 74 subjects without DD. Experiments were performed at 250 Hz and 500 Hz at the fingertip and palm. The VPTs were statistically analyzed with respect to disease status, age, gender, location tested, and frequency tested. We found that VPT increase with age, which agrees with findings by others. Women showed greater sensitivity (i.e. lower VPT) than men. Men exhibited lower sensitivity in DD vs. healthy subjects, but the results were not statistically significant. In subjects with DD presenting unilaterally, the unaffected hand was more sensitive than the affected hand, in particular for a 250 Hz stimulus applied to the finger. The data on vibration sensitivity obtained from a large group of subjects with and without DD presents interesting trends that may serve as a useful reference to future

DD researchers. Understanding additional symptoms of DD may facilitate development of novel diagnostic or prognostic protocols.

3.2 Introduction

Dupuytren disease (DD) is a progressive fibroproliferative disorder of the palmar fascia with characteristic nodules and cords [30]. Its incidence has been estimated at approximately 3 cases per 10,000 adults [32], with higher prevalence in individuals of Scandinavian descent [102]. Fibrobasts proliferate and differentiate into myofibroblasts, which produce collagen and exhibit higher contractility, leading to progressive shortening and contraction of the cords [103]. The disease usually presents clinically after age 50, and the ring finger is most commonly affected [29]. Progression of DD is divided into three grades: Grade 1 has a thickened nodule and/or band in the palmar aponeurosis but no discernable contracture, Grade 2 presents as permanent contracture with flexion angle less than 60 degrees, and Grade 3 is flexion greater than 60 degrees [104, 28]. The progression is highly variable and unpredictable [105]. The etiology is unknown, and, although there is a strong genetic component, there is currently no genetic test for DD [103]. Available treatments include fasciectomy [106], needle aponeurotomy [107, 108], collagenase injections [109], and radiation [110].

Patients with DD have been found to exhibit structural changes in the Pacinian corpuscles (PCs) of the affected tissue [18, 45, 46, 47, 48, 49]. As cutaneous mechanoreceptors in the deep dermis and subcutaneous tissue, PCs are sensitive to pressure changes and vibration in the frequency range of 20–1000 Hz [7, 8, 111, 4, 6]. Structurally, PCs consist of concentric lamellae surrounding an RA II nerve ending [17, 18]; this structure acts as a high–pass filter and enables high sensitivity to vibrational stimuli via interconnected collagen fibers [6, 18]. Ehremantant et al. reported that PCs from subjects with DD exhibited larger size and more numerous lamellae. The mean area of PCs from non–DD subjects was $1.0 \pm 0.5\, mm^2$, whereas the mean area of the PCs from subjects with DD was $2.6 \pm 0.4\, mm^2$ ($p \leq 0.001$); the number of layers increased from 40 ± 9 in subjects without DD to 64 ± 14 ($p \leq 0.01$) [47]. Given the PC's role in vibrotactile sensing, one may ask whether the structural changes associate with perception changes.

To estimate the effect of the more lammellated and larger PCs, the frequency of peak sensitivity was calculated based on our previous theoretical analysis [112]. Using a lamellar modulus of 1 kPa [27, 59, 58, 113], interlamellar fluid viscosity of 1.4 mPa·s [59, 58], lamellar thickness of 0.35 μm, outer radii of 0.56 mm and 0.91 mm [47], and number of lamellae of 40 and 64 for healthy PCs and DD–associated PCs, respectively [47], we calculated a peak frequency of 264 Hz for healthy PCs and of 833 Hz for those with DD. In the same

model, increasing the number of lamellae causes a decrease in overall threshold amplitude [112]. Based on those estimates, we hypothesized that subjects with DD would have reduced sensitivity, or higher VPT, at the affected fingers/palms compared to healthy controls and that the reduced vibrosensitivity in the subjects with DD to be more prominent at 250 Hz, where the healthy subjects are the most sensitive. Vibrotactile perception thresholds (VPT) have been studied in the healthy population [114, 115, 116, 117, 118, 119, 120, 121] and have been used to evaluate clinical neurology [122, 123, 124, 125], but the vibrotactile sensitivity of people with DD has not yet been investigated. Therefore, we conducted a study comparing VPT in healthy subjects vs. DD patients under different stimulus frequencies and locations.

3.3 Materials and Method

3.3.1 Patient selection

All the patients gave informed consent before the experiment and gave consent to publish the data. Vibration sensitivity was measured in 74 healthy volunteers and 36 subjects diagnosed with DD. Most of the healthy subjects were tested at the Driven To Discover Research Facility at the 2018 Minnesota State Fair. With assistance from the Fairview Research Administration, the majority of the subjects with DD were identified as recent patients (seen within 3 years) of the University of Minnesota or Fairview Clinics, aged between 60 and 70 years old and having a diagnosis of DD at any stage. Subjects with Raynauld's disease, peripheral neuropathy, or diabetic neuropathy were eliminated because they were expected to have non–Dupuytren–related lack of sensitivity. Subjects were recruited via letters and tested at the University of Minnesota in a private conference room. The experiments were IRB–approved (IDs: 1605M87741 and STUDY00002660) and were performed under IRB guidelines by a CITI–trained investigator.

3.3.2 Experimental device

The oscillating force probe used to measure palm/finger sensitivity at various frequencies is shown in Fig. 3.1. Vibrotactile stimuli were delivered with an 8.9 mm diameter piezoelectric disk bender (AmericanPiezo 20-1330) wired to a digital–to–analog signal generator (Syscomp WGM-201 or CGR-201, Ontario) and amplification system (Gemini XGA-3000, New Jersey). The normal force applied to the palm/finger needed to be normalized for all subjects because the sensitivity depends not only on the oscillation frequency and amplitude but also on the static normal force used during the application. The normal force was therefore measured and displayed during the device operation so that it could be maintained

at a desired value by the experimenter manually adjusting the stand. The normal force was measured via the pressure inside a chamber whose volume changes with applied force. As seen in Fig. 3.1c, the deformable portion of the device compresses the deformable area, resulting in a change in the pressure in the chamber. The pressure inside the chamber was measured in real-time using the barometer chip LPS25HB. The barometer chip has a sensitivity of 0.01 mbar, leading to the overall device having a sensitivity of 0.0154 (N/mbar) and a high resolution of 1.5x10-4 N in terms of force measurement. The pressure sensor and the vibrating piezo were both controlled via an in–house code. The device was designed in Autodesk Inventor and fabricated using the Stratasys J750 PolyJet 3D printer (14 μm layer accuracy). The flexible part of the probe that deforms to compress the entrapped air inside is made of Agilius Clear (Shore 60A), and the hard body of the probe is made of Vero White.

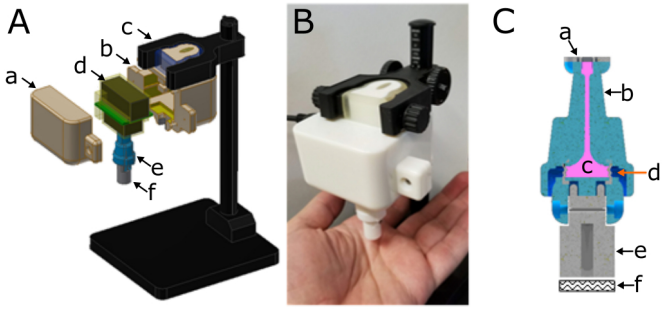

Figure 3.1: The probe used to measure vibrosensitivity. (A) Schematic design of the pneumatic force sensor: a the front cover, b the back cover, c the adjustable boom, d electronics, e pneumatic force sensor, f piezo holder. (B) Testing the fabricated device on a palm. (C) The force sensor's structure: a the location of the barometer, b the solid body, c compressed air in empty chamber, d deformable area, e piezo holder, f piezo.

3.3.3 Experimental study design

The subject was seated and placed his or her hand/finger in the device under the vibrating probe with his or her arm comfortably supported. The hand was tested at the distal palmar flexion crease and the center volar pulp (Fig. 3.2). The vibrating probe was lowered on the adjustable boom until the force sensor reached 0.5 N. After the device was in place, the subject received instructions through a graphical user interface (GUI) on a tablet computer and gave all responses via the computer's touchscreen, with the examiner remaining present to adjust the sensor as needed and to aid in transitioning between the locations tested. There were two locations tested—fingertip and palm—and two frequencies tested—250 Hz and 500 Hz. The order of locations was the subject's choice, and the order of the frequencies was selected randomly. At each frequency, the subject was presented with a continuous stimulus

and asked whether s/he felt the vibration. Amplitudes were adjusted according to a psi–marginal adaptive algorithm [126], in which the amplitude of each stimulus was increased or decreased based on the responses already received to produce a rapid estimate of the VPT. Each frequency was tested with 30 individual trials (Fig. 3.3). Before recording the responses, there were four practice trials where the stimulus was either at the maximum vibration amplitude (10 μm) or not vibrating; during this practice phase, the subject was told of the stimuli on the GUI and, in most cases, verbally by the examiner to confirm that the subject understood the experiment. The subject could redo the four practice trials if desired. Including completing the consent form and a brief explanation of their results by the examiner, the entire procedure took 15 minutes for healthy subjects, who were only tested on their dominant hand. Subjects with DD who came to the University of Minnesota were tested on both hands and, in many cases, multiple fingers; the experiment took an average of one hour with several breaks to rest and to discuss their medical history with respect to DD.

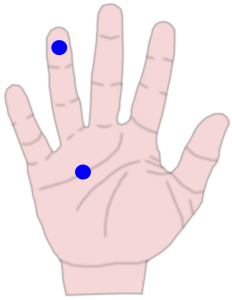

Figure 3.2: The hand was tested at the distal palmar flexion crease and the center volar pulp.

The amplitudes and responses for each trial were recorded, and the psi-marginal adaptive algorithm calculated a final threshold and standard error value. The majority of the data gave a clear threshold value as in Fig. 3.3A and were used for analysis without adjustment; there were, however, three scenarios that were deemed failures and eliminated or required additional analysis. The first failure case occurred when the subject selected that they could feel the vibration for two or more trials when the amplitude was zero, i.e. no vibration was present (Fig. 3.4A); this was likely due to the subject misunderstanding the experimental question or due to the subject misreading the response buttons. The second failure case occurred when the final standard error of the threshold was greater than 4 μm (Fig. 3.4B); this was likely due to the subject moving during the experiment and re–positioning the probe at a different location, due to the subject becoming distracted during the course of the experiment, or due to the subject not selecting the true response. The third failure was the inability to sense the vibrations at the maximum amplitude (Fig. 3.4c). Data

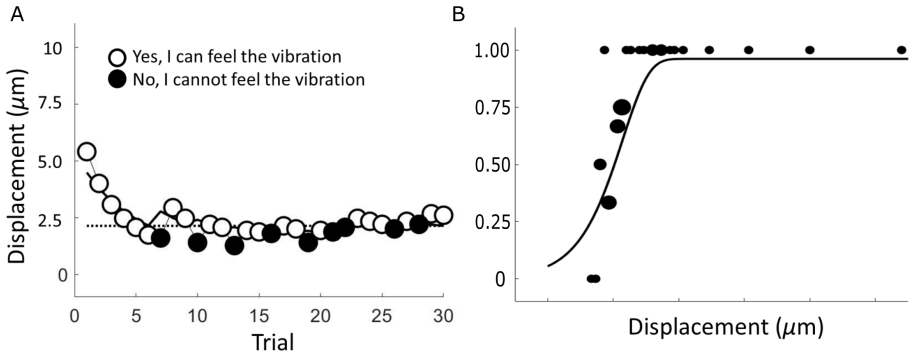

Figure 3.3: Examples of responses with the Psi–marginal adaptive method. (A) Example stimulus and responses. The open circles show where the subject selected that he or she could feel the vibration for each of the 30 trials. The filled circles indicate where the subject selected that they could not feel the vibration. The dotted line in the final threshold value calculated with the Psi–marginal adaptive method. (B) The dots indicate the likelihood of the same subject's response. A value of 1 corresponds to "Yes, I can feel the vibration" while 0 corresponds to "No." The size of the dot correlates to the number of individual trials at that amplitude. The line is the best–fitting Weibull probability function.

associated with the first and second cases of failure were eliminated from further analysis; data associated with the subject's inability to sense the vibration at maximum amplitude were treated as right–censored data and recorded as an amplitude of 10 μm.

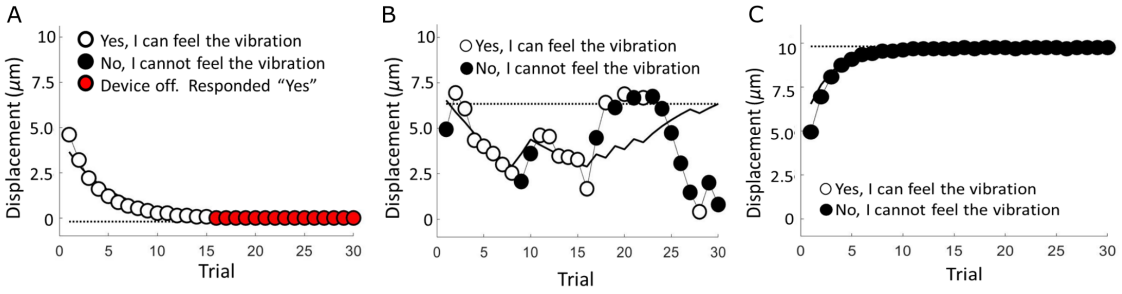

Figure 3.4: Examples of failed and censored experiments. (A) The subject selected that he or she could feel the vibration when the device was off and not vibrating. (B) The calculated error in the threshold is greater than 4 um. (C) The subject could not feel the vibration.

3.3.4 Statistical analysis

The data were manually sorted to eliminate the tests that were deemed failures. There were some data from subjects with DD on their non–clinically–presenting hands (e.g. they have a cord on their right ring finger but their left hand appears unaffected by DD); these data were temporarily removed from the larger analysis and analyzed separately. The remaining data were grouped by gender and DD status (data provided in the repository).

The mean VPT was calculated on a log–normal scale with an in–house code applying a tobit model that accounted for the censored thresholds. The model calculated a linear regression of the log of the VPT with respect to age for the healthy subjects. Additionally, the mean VPT from subjects over 50 years old was calculated for data from subjects with and without DD. An ANOVA was performed to determine the effects of the four groups: location (fingertip vs. palm), frequency (250 Hz vs. 500 Hz), gender (male vs. female), and DD status (non–DD vs. clinically presenting DD). Ad–hoc T–tests were performed for each comparison with an in–house code. For the subjects who had DD and were tested on their non–clinically–presenting hands, a one–way repeated measures ANOVA was calculated [127] and the difference in VPT was calculated with paired T–tests using the standard deviation from the Psi–marginal algorithm. All statistical comparisons were made with two–tailed tests.

3.4 Results

The dataset included 36 cases (14 male and 22 female) of DD and 74 cases (31 male and 43 female) of controls. The age distribution for the different groups are is provided in Fig. 3.5. The thresholds fits for the data from healthy subjects are shown in Fig. 3.6. The slope of the tobit fits for healthy subjects are similar for both frequencies and both locations, and the VPT increases with age.

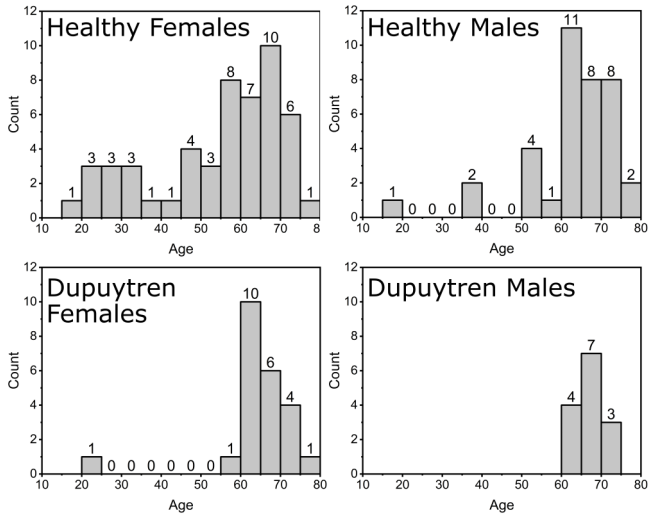

Figure 3.5: Histograms of the age distribution of all subjects.

The individual VPTs and fits are provided in Fig. 3.7. The mean and standard error of the data for subjects above age 50 separated by gender and DD status are shown in Fig. 3.8. When the data were analyzed by ANOVA, no effect (disease status, frequency,

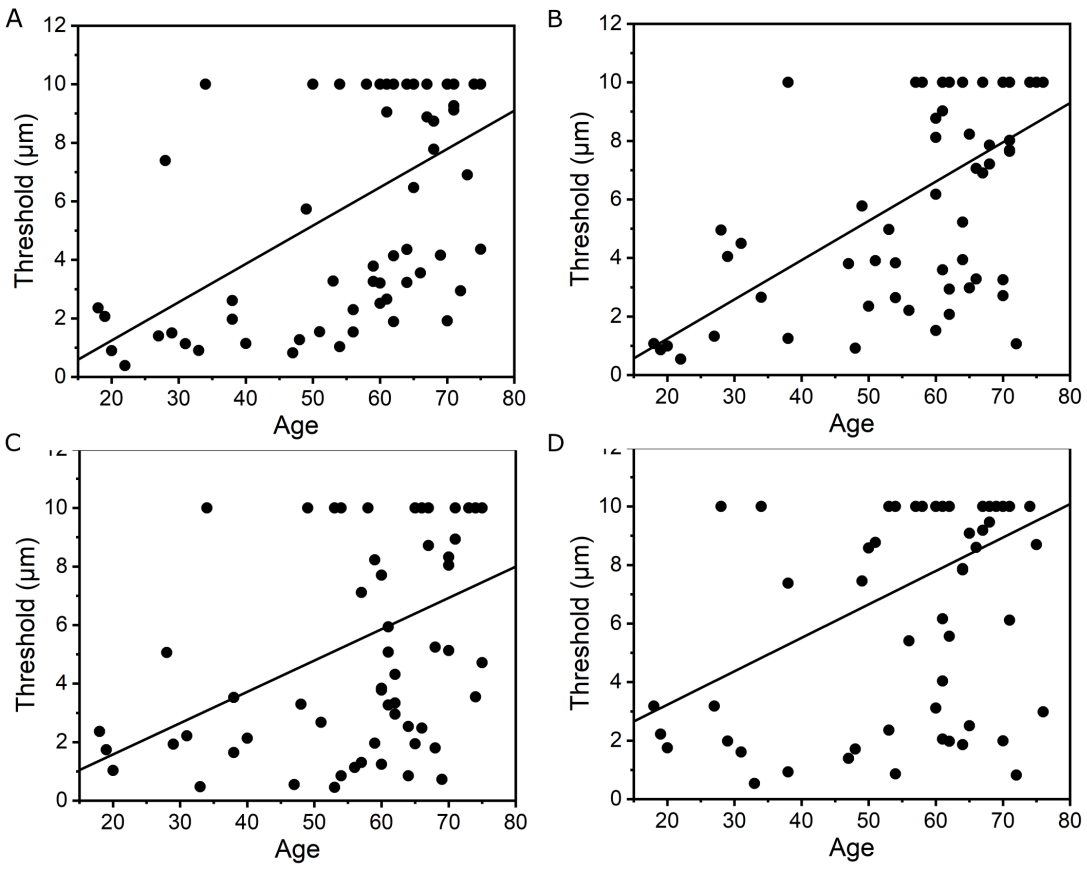

Figure 3.6: Threshold data for healthy subjects at (A) all ages at 250 Hz at the fingertip, (B) 250 Hz at the palm, (C) 500 Hz at the fingertip, and (D) 500 Hz at the palm. The lines were calculated by tobit analysis.

locations, or gender) had a significant influence on VPT for either the ring finger only ($F(15, 247) = 0.81, p = 0.67$) or for all the fingers combined ($F(15, 344) = 1.09, p = 0.36$). When each effect was investigated separately in a multi–way ANOVA, gender affected the VPT ($p_{sex,\,ring} = 0.02, p_{sex,\,all} = 0.01$), but no other group had a significant effect ($all\,other\,p > 0.1$). The differences in gender are visible in Fig. 3.8 and appear to be exaggerated in the DD subjects.

The paired VPT of subjects with unilaterally clinically–presenting DD are shown in Fig. 3.9. The hand with DD is less sensitive than the unaffected hand for 250 Hz on the fingertip ($F(1, 16) = 6.29$, $p_{250\,Hz\,fingertip} = 0.037$), but the trend is less consistent for the other frequencies and locations ($H(1, 16) = 0.35, p_{250\,Hz\,palm} = 0.35, F(1, 14) = 0.56, p_{500\,Hz\,fingertip} = 0.48, F(1, 16) = 0.028, p_{500\,Hz\,palm} = 0.87$).

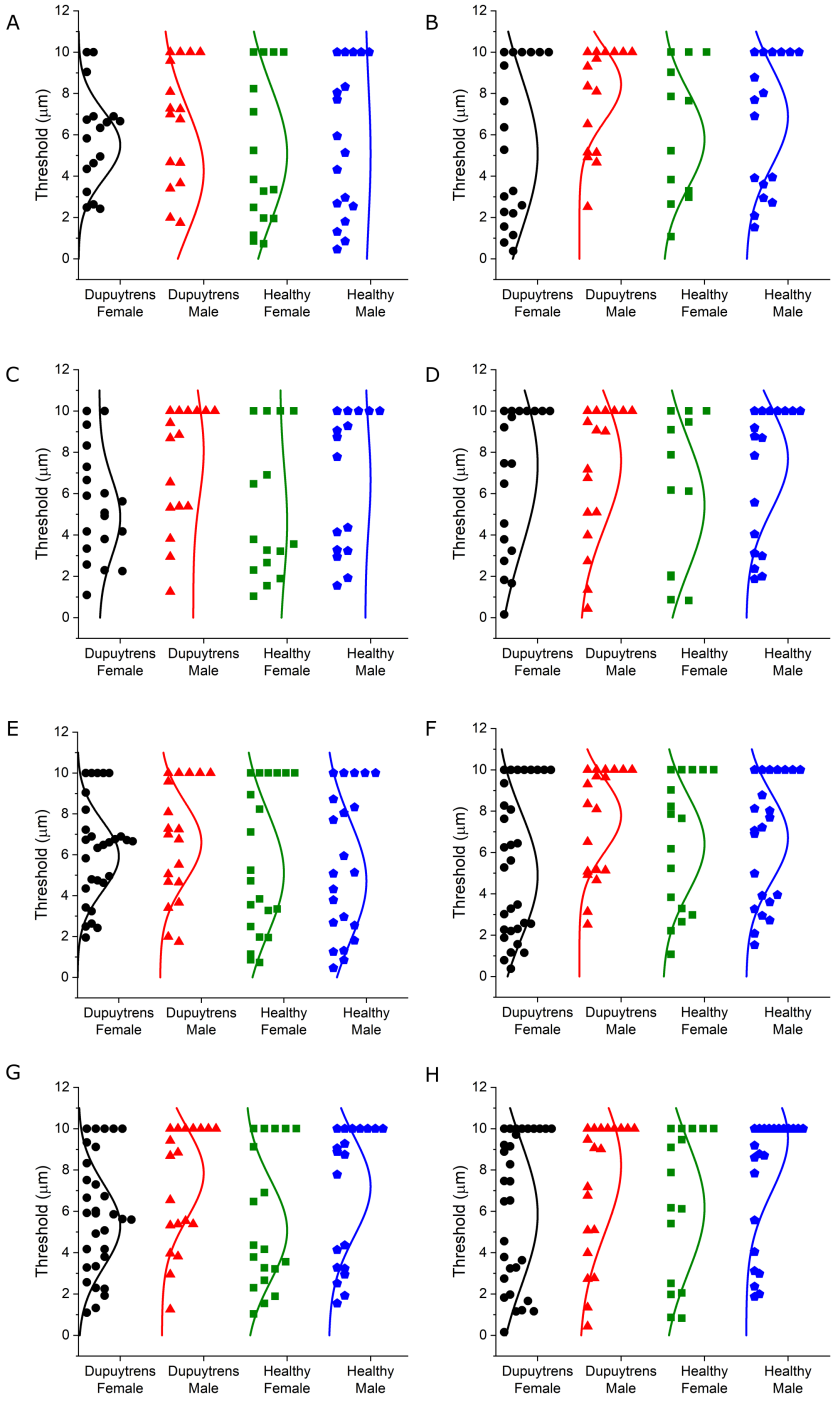

Figure 3.7: Thresholds of subjects over 50 years old for the ring finger only at 250 Hz at the fingertip, (B) 250 Hz at the palm, (C) 500 Hz at the fingertip, and (D) 500 Hz at the palm, and (E) for all the fingers combined at 250 Hz at the fingertip, (F) 250 Hz at the palm, (G) 500 Hz at the fingertip, and (H) 500 Hz at the palm.

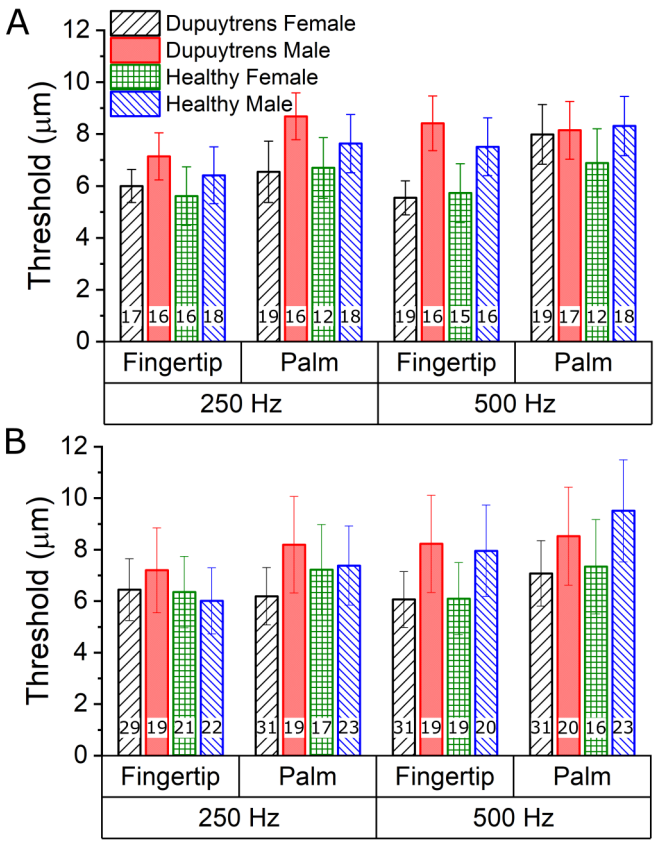

Figure 3.8: Threshold and standard error values (A) for the ring finger and (B) for any finger.

3.5 Discussion and Conclusion

In this study, we tested whether subjects with DD have reduced and/or shifted vibrosensitivity at the location of the affected fingers and palms compared to healthy controls. We also investigated the effects of age and gender. Our key findings are as follows:

- As found previously by others [111, 128, 129, 130, 131, 132, 133, 134], VPT increased with age
- Women showed greater sensitivity (i.e. lower VPT) than men (($p_{sex,\,ring} = 0.02$, $p_{sex,\,all} = 0.01$))
- Men exhibited lower sensitivity (i.e. higher VPT) in DD vs. healthy subjects, but the results were not statistically significant ($p_{male,\,ring} > 0.4$, $p_{male,\,all} > 0.15$)
- In subjects with DD presenting unilaterally, the unaffected hand was more sensitive than the affected hand, in particular for a 250 Hz stimulus applied to the fingertip ($p_{250\,Hz\,fingertip} = 0.037$))

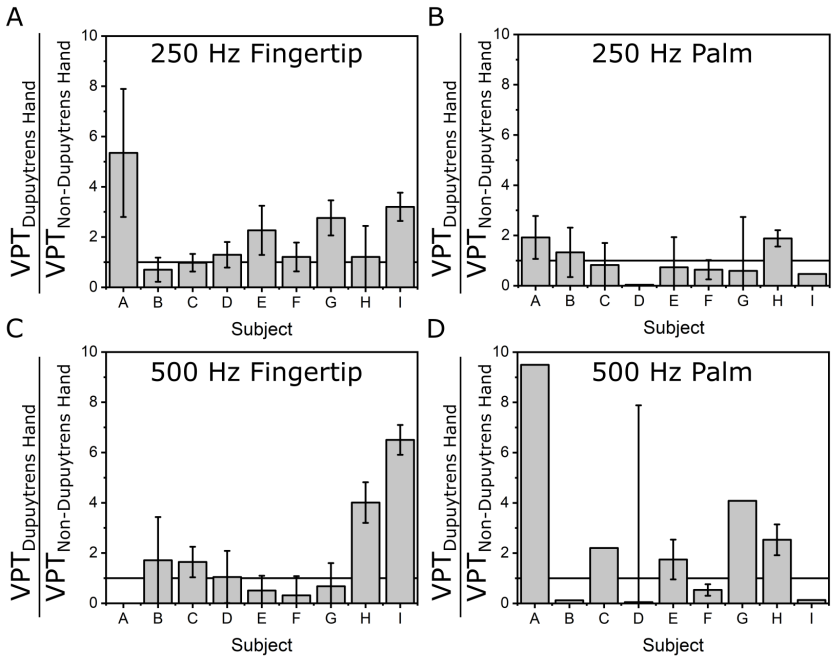

Figure 3.9: Paired data for each subject with the ratio of the VPT of the Dupuytren hand against the hand that does not have clinically–presenting DD. The threshold and relative standard deviations for separate subjects A-I are shown for (A) 250 Hz fingertip, (B) 250 Hz palm, (C) 500 Hz fingertip, and (D) 500 Hz palm. A value greater than 1 indicates a relative lack of sensitivity in the affected hand.

These results are discussed in further detail below.

The VPT of healthy subjects decreased with age at all frequencies and locations tested (Fig. 3.6). This result is consistent with previous studies [111, 128, 129, 130, 131, 132, 133, 134]. The reduced sensitivity is believed to be caused by degenerative changes in PCs (e.g. demyelination) as well as changes in the central nervous system.

The measured VPTs were different between men and women with women in the same age range showing greater sensitivity to vibration (Figs. 3.7 and 3.8). A sensitivity difference with gender was reported by Peters et al. [135] and explained by women having smaller fingers and, therefore, a higher density of a related mechanoreceptor, the Meissner corpuscle, although Peters et al. tested passive spatial tactile acuity and not vibration sensing. As shown in Figs. 3.7 and 3.8, the male subjects with DD exhibited slightly lower vibrosensitivity than the healthy controls under all conditions except 500 Hz at the palm, yet this effect fell within acceptable error.

A notable feature of all our experiments was the very wide scatter of the data. Individual experiments were reproducible and gave small error estimates, but the population showed considerable variability. This variation is not surprising given the many factors that could confound the experiment, discussed in the following paragraph, but it presents

a considerable challenge. The observable trend in the paired study vs. the cross–sectional study emphasizes the importance of individual variability and suggests that a longitudinal study could be more informative.

First, we consider variability arising from our testing system. The force applied to the finger/hand by the probe was maintained at 0.5 N, but variations in individual finger dimensions, fat vs. muscle content, and tissue stiffness could all affect that force and vibration sensing differently, leading to variation in the measured result. Also, although our probe is fairly large (8.9 mm diameter) and thus is expected to fall within the receptive fields of many PCs [14, 15, 16, 5], the vibrational signal attenuates through the skin [99, 136, 63], so the exact location of the PCs within the finger or hand being tested—which is obviously unknowable—would affect the measured sensitivity. Finally, it is noted that within an individual, there is wide variation in PC properties [53], which would also lead to more variability in our measurements.

The individual subjects who had clinically–presenting unilaterally DD exhibited higher VPTs at 250 Hz on the fingertip. However, the trend did not continue at the other frequencies and locations (Fig. 3.9); a few subjects showed VPT trends opposite from what was expected (e.g. 3 of the 9 had lower VPTs in their DD hand at 250 Hz on the palm), and there were some large discrepancies (e.g. several of the subjects could not feel the 500 Hz vibration on their palm with either hand). It is possible that the PCs on the subjects' affected hand are not different from the other hand, or, conversely, it is possible that the subjects have enlarged PCs on both hands but have not yet developed nodules or cords on their non–clinically–presenting hand. A longitudinal study is needed for more definite conclusions.

There are several factors for which this study does not account but which may affect the vibrosensitivity. Firstly, the subjects had different stages of DD; some subjects had minor nodules on a single finger (stage I) whereas others had contracture greater than 90 degrees on several fingers (grade III). Secondly, the subjects had different treatments; some subjects had surgery or collagenase injections to one or multiple fingers. Thirdly, some subjects had particularly aggressive forms of DD; there is currently no measurement of aggressiveness in DD, yet some subjects claimed that they had surgery and the cords and contracture returned within months whereas other subjects stated they have not noticed a change since diagnosis. Finally, although any volunteers who stated that they have peripheral nerve disorders were eliminated from the study, it is possible that there were subjects with undiagnosed neuropathy. It is possible that the PC growth, and therefore subsequent changes in vibrosensitivity, may be related to the stage, treatment, or aggressiveness of DD. A longitudinal study would be required to investigate these effects.

Chapter 4

Viscoelastic properties of the Pacinian corpuscle

The content of this chapter is still in preparation. Only preliminary findings are reported. The current author list is: Tiffany L. Senkow, Emily A. Chandler, Amy T. Moeller, and Victor H. Barocas.

4.1 Summary

Although Pacinian corpuscles (PCs) respond to high–frequency vibratory stimuli in the range of 50-1000 Hz, the viscoelasticity of the PC has not been studied under dynamic stimulation. In this chapter, we studied the viscoelastic properties, chiefly the Young's modulus and the viscosity, of the PC at physiologically–relevant timescales. We created a cantilever-based device and an equivalent computational model that stimulated the sample and measured the resulting waveform that passed through the sample and the cantilever. By calculating i) the displacement at the cantilever above the sample and ii) the phase shift between the cantilever's motion and the input vibrations at a range of frequencies for both the device and the simulation, we could optimize the parameters for Young's modulus and viscosity. Analysis of ∼100 PCs from three donors are current ongoing, but preliminary findings on a representative isolated human cadaveric PC had a Young's modulus of 84 Pa and viscosity of 0.84 Pa·s. Using donors with and without Dupuytren disease (DD), we could investigate whether there were differences in the size or viscoelastic properties of the PCs. The PCs from a human cadaveric donor with DD were significantly larger than the PCs from two donors without DD, although it would not be appropriate to draw conclusions about PC changes in DD based on only on three donors.

4.2 Introduction

4.2.1 Pacinian corpuscle

Pacinian corpuscles (PC) are cutaneous mechanoreceptors primarily located in the glaborous (i.e. non-hairy) skin [7]. There are approximately 300 PCs in the human hand [53]. They are sensitive to pressure changes and vibrations in the high–frequency range (approx. 40-1000 Hz) [7, 8, 9, 4, 6]. In the human hand, PCs can detect objects' texture [10, 11, 12] and are responsible for fine control of tools [4]. PCs are most sensitive to stimuli around 250 Hz [9, 137].

PCs are ellipsoidal in shape with dimensions on the millimeter scale [18]. Structurally, they have a central type II rapidly–adapting (RAII) terminus with an inner layer of tightly–packed lamellae [7, 18, 138, 17]. Lamella, especially in the inner core, are composed of non–neuronal squamous epithelial cells [24, 139]. Moving radially outward, the lamellae, comprising about 30 layers of modified perineural epithelial cells, become more spaced apart [18, 7, 24, 17]. The layers are separated by fluid [20] and contain collagen fibrils and bundles that have dominant circular organization around the central neurite [17, 7]. Collagen is proposed to serve as a support mechanism, and it is believed that the density of collagen within the PC increases with age [18]. Due to the unique structure and the interaction between fluid and lamellae, PCs act as bandpass filters, transducing vibratory stimuli from the outer shell to activate the central afferent nerve [4, 25, 8].

4.2.2 Viscoelasticity

There have been several *in silico* biomechanical models of the PC since the initial work of Loewenstein and Skalak [27, 59, 113, 63, 58, 62]. The models include estimates for the viscoelastic parameters with Young's modulus ranging from 1 kPa [59] to 500 kPa [27] and viscosities similar to those of water, $\sim$1 mPa·s [27, 59, 113, 63, 58, 62]. Quindlen et al. began to address the lack of measured parameters by using micropipette aspiration on isolated, cadaveric human PCs [64]. They calculated an apparent Young's modulus of 1.4 $\pm$ 0.86 kPa under steady–state conditions [64]. To date, no study has investigated the viscoelastic mechanical parameters of the PC at physiologically relevant timescales where the PC is responsive.

4.2.3 Dupuytren disease

Dupuytren disease (DD) is a progressive fibroproliferative disorder of the palmar fascia [30]. The disease is characterized by shortening and thickening of fibrous bands in the hands in the fingers. Elevated, hard regions of fibrous tissue are called nodules are often

located in the palm. Fibrous bands, called cords, may extend into the fingers [33]. In many cases, the nodules occur first followed by cords, which can cause permanent flexion contracture of the affected fingers [140, 28]. Contracture of the metacarpophalengeal and proximal interphalangeal joints occurs over months to years, with the progress being highly unpredictable [105]. Severe contracture can restrict hand function and diminish quality of life. In the United States, the estimated incidence, including both physician diagnosis and self–reported symptoms, is 7.3% [32], and the majority of people with the disease are over the age of 50 and of Northern European descent [102, 140]. The cause and mechanism of progression are unknown [33, 140], although there is a genetic disposition [141].

The formation of the Dupuytren nodules and cords is likened to connective tissue wound repair [142]. In DD, fibroblasts proliferate and, as in wound healing, differentiate into myofibroblasts, subsequently forming the cords. These myofibroblasts produce collagen I and III, leading to higher contractility that is responsible for the contracture [103, 142, 103]. Genes for the production of collagen I, V, and VIII were found to be upregulated in tissue with DD compared to control palmar fascia [38].

4.2.4 Study Objectives

Values for the elasticity and viscosity of the PC determined by mechanical stimulation would improve the accuracy of computational models of the PC. The first goal of this study is to determine the viscoelastic properties of the PC by testing at physiologically relevant timescales, i.e. in the 50-500 Hz range. Secondly, compared to PCs from healthy subjects, PCs extracted near the nodules and cords of subjects with DD have been reported to be larger [47, 46, 45, 49, 50, 51], to have more numerous lamellae [47], and to have more collagen [50]. Based on these changes, one would predict a change in the viscoelasticity of PCs near Dupuytren nodules and cords. The second goal of this study is to compare the size and viscoelastic properties of the PCs from healthy donors to PCs from donors with DD.

4.3 Methods

4.3.1 Device

We designed a system (Fig. 4.1) to stimulate an isolated mechanoreceptor mechanically from beneath and to measure the displacement of the PC on the opposite (i.e., top) surface. The base of the apparatus consisted of a flat piezoelectric disc bender (APC International, Ltd. 20-1330). Vibrational stimuli were delivered to the piezo via the waveform generator function of a multifunction oscilloscope (CGR-201 with Unified CircuitGear Software, On-

tario) and amplified (Genimi XGA-3000, New Jersey) to 30 V, the maximum input voltage of the vibrating piezos. At 30 V input voltage, the pieozos vibrated with a displacement amplitude of 10 μm. The sample was placed directly on top of the piezo. A polystyrene cantilever was mounted on an adjustable holder and lowered until it contacted the top of the sample. Upon sample stimulation, the response motion of the cantilever was recorded via a laser vibrometer with an interferometer (Polytec, OFV-2600/OFV-352). The input waveform to the piezo and the vibration recordings from the interferometer were recorded simultaneously with the oscilloscope. We tested frequencies from 30 Hz to 500 Hz in increments of 5 Hz. Approximately 30 periods were recorded at each frequency with a minimum sampling frequency of 10,000 Hz.

The input waveform to the piezo and the simultaneous output waveform from the laser vibrometer were were characterized with Fourier analysis and fit to sinusoids with the frequency of the input stimulus, ω:

$$Asin(\omega t + \phi) \tag{4.1}$$

The displacement was determined from the amplitude, A, of the cantilever. At each frequency, the overall phase shift was calculated as $\phi_{cantilever} - \phi_{piezo}$. Because some frequencies did not produce clear response waveforms, any sinusoidal fit with an R–square value less than 0.9 was eliminated from further analysis. The device was characterized with polydimethylsiloxane (PDMS, nearly elastic) and silicone oil (viscous).

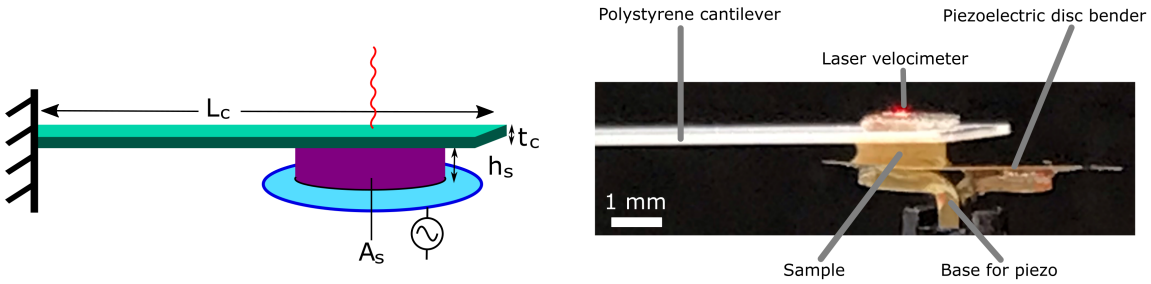

Figure 4.1: Measurement device. The sample lies between the vibrating piezo and the cantilever. The cantilever length, L_c, cantilever thickness, t_c, sample height, h_s, and cross sectional area of the sample, A_s, are shown on the schematic on the left. Cantilever deflection at the center of the sample was measured with a laser interferometer. The right shows a photo of the device with silicone oil as the sample.

4.3.2 Specimen preparation and testing

The University of Minnesota Anatomy Bequest program provided human cadaveric hand specimens for PC collection. There were three donors: non–Dupuytren female aged 92 left

hand, non–Dupuytren male aged 86 left hand, and Dupuytren male aged 93 right and left hands. PCs were identified and isolated from the proximal phalanx and the metacarpal head as described previously [64]. Samples were placed in 100 IU/mL penicillin and 100 μg/mL streptomycin in PBS and temporarily stored at 4 °C after isolation and between tests. The length of the long and short axes of the PCs were measured before testing. Some of the heights of the PCs were measured while in the device with the cantilever in place; the ratios of the height compared to the long and short axes were calculated, and these ratios were used to calculate the height of the remainder of the PCs. We were unable to collect data for the four smallest PCs because they could not be reliably placed in the device. Individual PCs were tested at room temperature, and a small volume of PBS was applied to the PC's surface with a needle syringe as needed to maintain sample hydration. Each experiment took 15-20 minutes. All the tests were completed within 3 days of dissection.

4.3.3 Finite–element model

We created a finite–element model of the measurement device in COMSOL Multiphysics to optimize the viscoelastic parameters using the displacement and phase shift measurements calculated from the vibrating device (Fig. 4.2). The cantilever was modeled as a long, thin, flat cuboid with the same physical parameters as the cantilevers used in the physical system. The sample was modeled as a Kelvin–Voigt solid with a single spring and dashpot. The sample, modeled as a cylinder, with the individual diameter from the long axis and the height from the measured or the calculated height. The 10 μm amplitude sinusoidal displacement in the z–direction was applied directly to the base of the sample, thereby eliminating the need to include the piezoelectric disk in the finite–element model. The displacement in the z–direction and the phase were measured on the cantilever directly above the center of the sample, i.e. at the location of the laser on the physical device, and the base of the sample was used a reference for the phase shift.

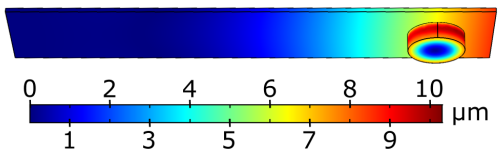

Figure 4.2: Harmonic displacement of the model. The thin rod is the polystyrene cantilever and the cylinder is the model. The sinusoidal stimulus is applied directly to the base of the sample.

4.3.4 Model optimization

The MATLAB *fminsearch* routine was used to identify the two parameters (Young's modulus, E, and viscosity, η) using the Nelder–Mead simplex method. The objective function for the optimizer was the sum square error (SSE):

$$S = W[x_{sim}(\omega) - x_{device}(\omega)]^2 + [\phi_{sim} - \phi_{device}(\omega)]^2 \tag{4.2}$$

where x_{sim} and x_{device} are the displacement of the simulation and experimental device at each frequency, ϕ is the phase shift, and W is a weighing factor to reduce optimization bias from the different scales used for displacement and phase shift.

The fitting process involved choosing two parameter values (modulus, E, and viscosity, η) so that a finite–element simulation of the experiment matched the experiment as closely as possible based on the measured phase shift and vibration amplitude vs. forcing frequency plots. The challenge was that the finite–element model took considerable time to run ($\sim$ 10-15 minutes) and needed to be run multiple times for each fit, and, additionally, because of limits of the University's license, the simulations could not be run in parallel or for very long times (lest other users revolt!). We had to fit $\sim$100 samples, so an accurate initial guess was important to minimize run time. The method for selecting the initial guess is provided in the Appendix at the end of this chapter.

4.3.5 Statistical Analysis

The data on the sizes of the PCs were tested with two–sample T–tests at the 5% significance level using the Bonferroni–Holm correction for multiple comparisons [143]. All statistical comparisons were made with two–tailed tests.

4.4 Results

4.4.1 PC Sizes

The mean and 95% confidence intervals of the PC lengths along the long–axis are shown in Fig. 4.3. The PCs from the donor with DD was separated into four groups based on its location in the hand: i) unaffected index finger from the right hand, ii) unaffected index finger from the left hand, iii) left ring finger with visible contracture), and iv) right ring finger that underwent surgery to remove the Dupuytren–associated cord. The two donors without DD had similar sizes with mean lengths of 2.8 $\pm$ 0.2 mm and 3.0 $\pm$ 0.2 mm along the long axis and 1.8 $\pm$ 0.2 mm and 2.1 $\pm$ 0.2 mm for the short axis. The PCs from the donor with DD were significantly larger ($p = 0.0132$) than the PCs from the donors without

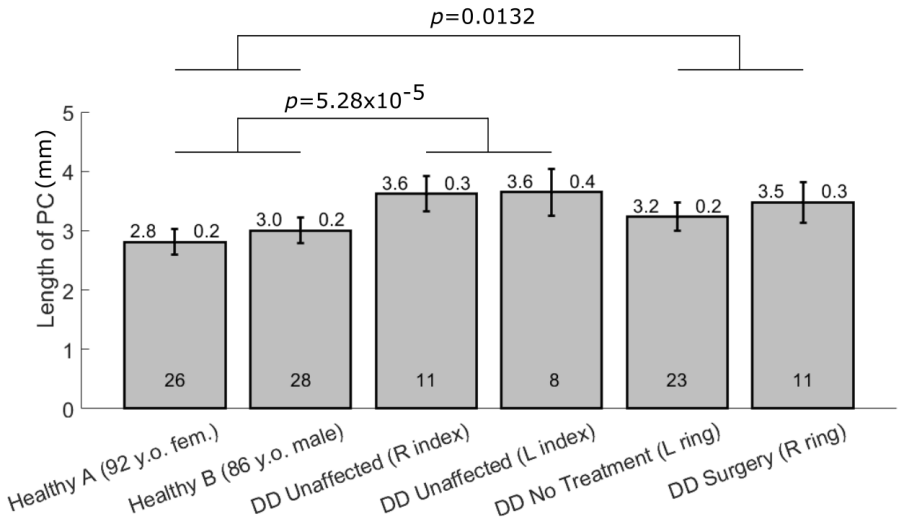

Figure 4.3: PC sizes. Mean and 95% confidence interval for the PC lengths measured along the long axis with the Bonferroni–Holm corrected p–values shown. The mean value is on above the bar to the left side with the the 95% confidence above the bar to the right side. The number of samples are listed at the base of the bars. p–values less than 0.05 are not shown.

DD. The PCs from the non–DD donors were smaller than the unaffected index fingers from the donor with DD ($p = 5.3 \times 10^{-5}$), although there are fewer samples from the index fingers of the DD donor. The size effects were more pronounced along the long–axis, with no statistically–significant difference observed in the shorter direction.

4.4.2 Characterization

The device was tested with PDMS, a nearly elastic sample. The displacement and corresponding phase shift observed for a the elastic sample with a cantilever of length 4 cm and width of 0.75 mm is shown in Fig. 4.4. According to the simulation, the peak displacement of the simulation results was 140 μm, located at 355 Hz (point C, out of bounds of the figure). Including the large displacement values, the SSE of the displacement was 6.9×10^4; when a cutoff displacement of 40 μm was enabled, the SSE displacement was 8.1×10^3. The right side of 4.4 shows the modal shifts that occur for select frequencies of interest.

The device was further characterized with viscous samples. Fig. 4.5 shows the resulting phase shifts and displacements with silicon oil of 200 mPa·s with two cantilevers: a length of 4 cm and thickness of 0.50 mm and a length and 8 cm and thickness of 1.0 mm. Measurements on the device were taken in triplicate. The displacements of the cantilever in Fig. 4.5 illustrate the resonance modes of the system.

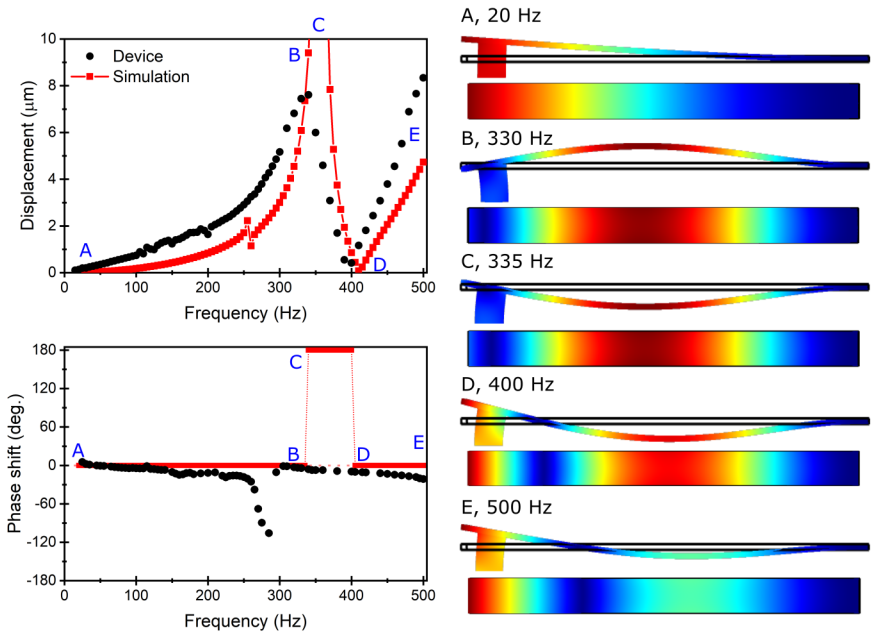

Figure 4.4: Characterization of the buzzing device with a nearly elastic sample. The displacement and phase shift of the device (black circles) compared to the simulation (red squares). The displacement of the cantilever for the five noted frequencies are shown to the right with cool colors denoting minimal overall displacement and warm colors denoting high displacements. The side view and the top vie of the cantilever are provided for each frequency. The side–view displacements are exaggerated by different scaling factors to visualize the overall displacement profiles and the resonance nodes.

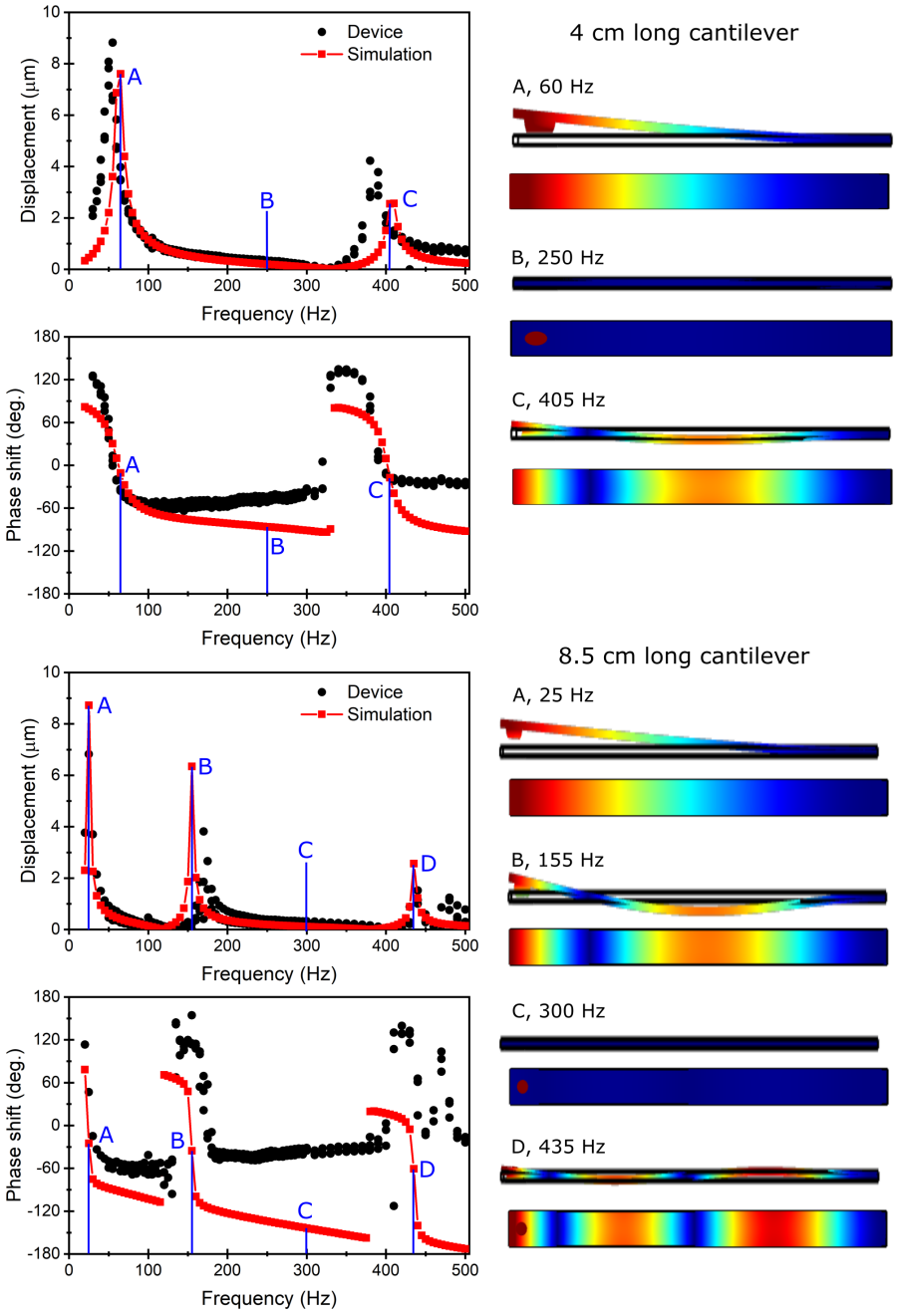

Figure 4.5: Characterization of the buzzing device with a viscous sample. *Top*) Displacement and phase shifts of a viscous sample (200 mPa·s) with cantilever length 4 cm and thickness of 0.5 mm from the device (black circles) and the simulation (red squares). Displacements at the noted frequencies from the simulation are to the right. Cool colors denote minimal overall displacement; hot colors denote higher displacements. The side and top views of the cantilever are provided for each noted frequency. The side–view displacements are exaggerated by a factor of 300. *Bottom*) The viscous sample with cantilever length 8.5 cm and thickness of 0.75 mm.

4.4.3 Viscoelasticity

A PC sample extracted from the donor with DD that was the average size from that donor was selected as preliminary PC data to further explore the system. All the PC data provided below are from this individual sample.

Waveforms of the piezo and cantilever were collected for 20 Hz through 500 Hz in increments of 5 Hz. Examples of the waveforms are provided in Fig. 4.6. The data were fit to sinusoidal waveforms with the known frequencies, and only the data with $R^2 > 0.9$ were analyzed further. The 330 Hz waveform in Fig. 4.6 is an example of a poor fit that was eliminated from analysis.

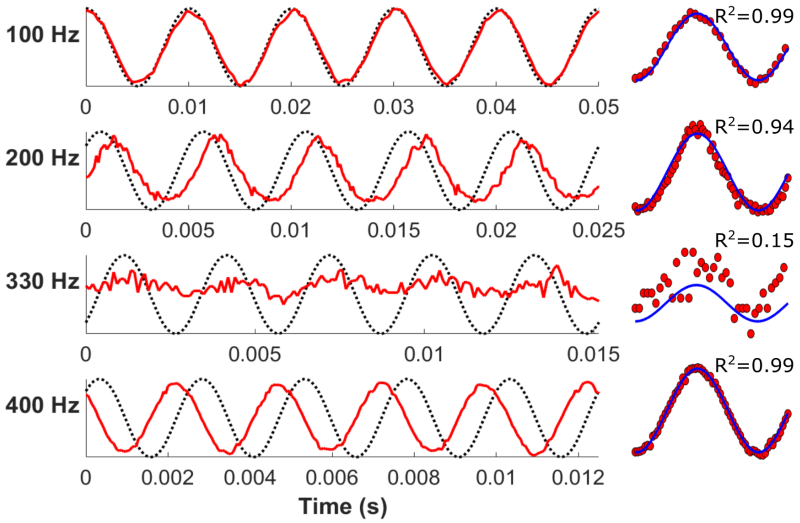

Figure 4.6: Representative experimental data. Left) The normalized piezo (black doted lines) and the normalized output from the cantilever (red solid lines). Right) The data from the cantilever (red dots) were fit to sinuoidal waveforms (blue solid lines). The R^2 values of the sinusoidal fit are shown; the 330 Hz waveform is an example of data that were eliminated from analysis due to poor fit.

The parameters for Young's modulus and viscosity were optimized by minimizing the SSE of the experimental and simulation data. For a better understanding of the acceptable bounds on the optimization, simulations were run for the representative PC with the same physical characteristics as the device (cantilever with length 3 cm and height 0.25 mm and the sample dimensions as measured) and with a variety of viscoelastic parameters. The plots of the SSE of the displacement and phase shift calculated independently and calculated with the weighted combination are shown in Fig. 4.7. The weighted combination was a multiplier factor of 100 applied to the SSE of the displacement. There was a band of lower error in the displacement around a Young's modulus of 100 - 500 Pa (Fig. 4.7A and 4.7D), and there was a band of lower error in the phase shift around a viscosity of 0.5 - 1 Pa·s (Fig. 4.7B

and 4.7E).

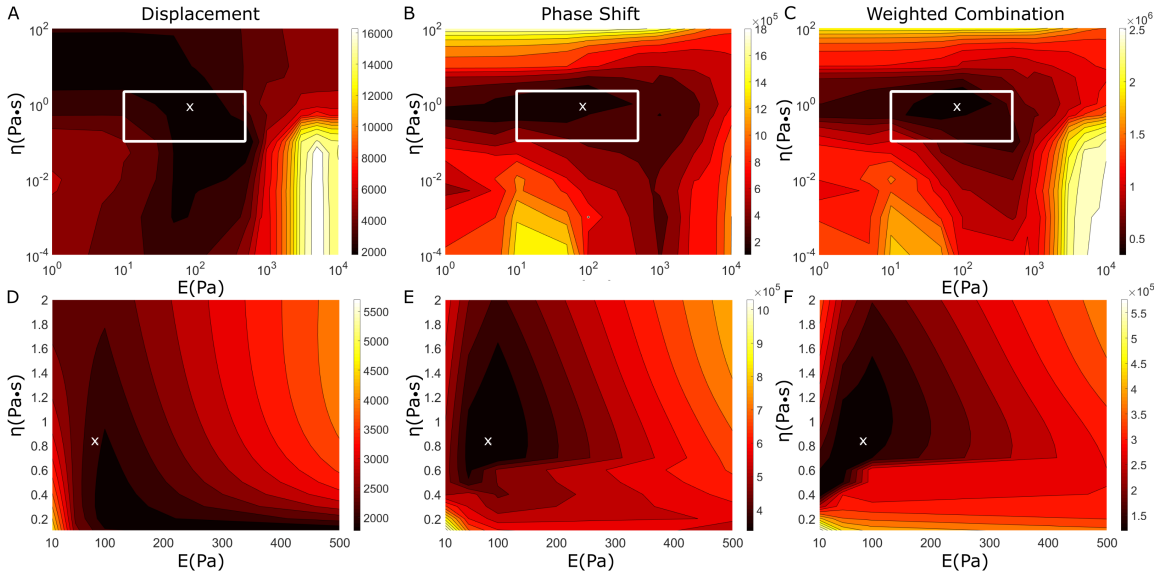

Figure 4.7: Example sum square errors of the simulation data compared to the experimental results of a) the displacement data, b) the phase shift data, and c) a weighted combination of displacement and phase shift. Zoomed contour plots of the SSE denoted in the white rectangles are provided in further detail in the bottom row in d, e, and f. The white x denotes the location of the best fit according to the optimization. Note the log plots in the top row and linear plots in the bottom row. The colorbar is re–scaled in each image for ease of visual analysis.

A representative example of data from the buzzing experiment and the simulation is provided in Fig. 4.8. The displacement vs. frequency plots all have two peaks around approximately 100 and 400 Hz and have some datapoints centered at ∼330 Hz that were eliminated from analysis due high errors of the sinusoidal fits.

Based on the data of the representative PC, the optimized parameter for the Young's modulus was 84 Pa and the viscosity was 0.84 Pa·s. The resulting displacement and phase shift curves are shown in Fig. 4.8.

4.5 Discussion

4.5.1 PC Sizes

Adult PCs are 3-4 mm in length [18]. It is believed that PC size increase gradually with age until approximately age 70, at which point the corpuscles become smaller [18, 7]. The age of the human donors were 86, 92, and 93, and, due to donor availability, only one donor had DD. The mean length of the healthy PCs was 2.9 mm, and the PC sizes ranged from 1.64 mm to 4.54 mm along the long axis, which agrees well with previous findings [53]. As

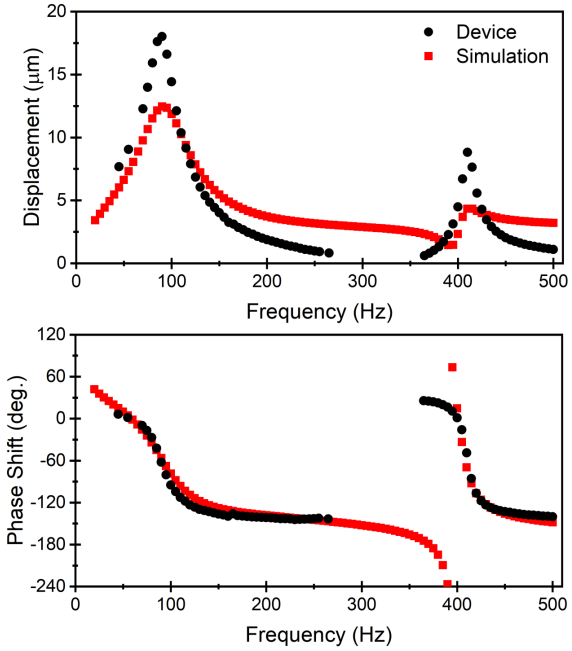

Figure 4.8: Representative best fit. The displacement (top) and phase shift (bottom) of the experimental (black circles) and simulation (red squares).

shown in Fig. 4.3, the PCs from the donor with DD were larger than the PCs from either subject without DD. This finding agrees with previous reports that PCs extracted near the cords of DD subjects are larger [47, 46, 45, 49, 50, 51]. There are other variables that may be partially responsible for the differences in PC sizes between donors including age, gender, body–size, occupation, and other diseases.

4.5.2 Characterization

The device was characterized with elastic and viscous samples. For the purely elastic sample, the simulation yielded no phase shift at most frequencies, which was expected; however, as shown in Fig. 4.4, there was a 180° phase shift in the simulation at the location where the slope of the frequency vs. displacement line was negative (i.e. 335-395 Hz). The maximum displacement of 140 μm at 335 Hz was well out–of–range of the laser velocimeter and represents an ideal theoretical scenario. In the simulation, the elastic sample and the polystyrene cantilever form a perfect union and could not break contact. If the device was placed with the solid, elastic sample directly against the beam, then there was contact loss at the resonance frequencies, which disrupted the system. To prevent the system from separating, the top of the elastic sample was coated with water or PBS to form a seal with the cantilever. The water introduced surface tension and some viscous components into the system that are not modeled, which may also partially explain the phase shift in the device

data seen around 300 Hz in Fig. 4.4.

A sample of silicon oil with known viscosity 200 mPa·s was tested. In a viscous sample (i.e. a Newtonian liquid), one would expect the phase shift to be 90°, however, as shown in Fig. 4.5, both the device and the simulation varied significantly from 90°. Each change in phase shift was accompanied by a peak in the displacement. The locations of these features differed with the length of the cantilever, the thickness of the cantilever, and the viscosity of the sample (the different cantilever widths were not tested). When the system was simulated with the same characteristics as the device, including a sample with viscosity of 200 mPa·s, the resulting displacement and phase shifts at each frequency followed the same trends as the device (left panels of Fig. 4.5).

The displacement profiles of the cantilever in the right panels of Fig. 4.4 and Fig. 4.5 illustrate the nonlinear, dynamic response of the system and the effects of the system's resonance. In an ideal scenario, the following events would occur to the system as the frequency is increased: At low frequencies, the system is below the first fundamental frequency and the entirely of the beam bends upwards with a maximum displacement at the free end (shown in 20 Hz in Fig. 4.4 and 25 and 60 Hz in Fig. 4.5). As the frequency increases, the natural frequency of the system is reached and the first resonance flexural node is formed. The second resonance frequency can be attained, producing a second node, as the frequency is increased. Continuing with increasing frequencies, more nodes occur in the system and the maximum displacement between the nodes is reduced. The progression of the resonance and the flexural nodes with respect to increasing frequency are visible in the right panel of Fig. 4.4 — with increasing frequencies, the location of the deep red indicating maximum displacement moves from the edge near the sample towards the bounded edge, and the deep blue stripe indicating the first flexural node shifts the same direction. The system with the 8.5 cm cantilever in Fig. 4.5 experienced three nodes.

At regions away from the flexural nodes, the phase shift of the viscous sample was linear with minor changes between frequencies (see Fig. 4.5), although the phase shift was not $\pm 90°$ as anticipated. The consistent phase shift in combination with the minimal displacement suggests that all the energy is being dissipated as heat, which is expected for purely viscous liquids, instead of being stored in the material, which is characteristic of elastic samples. The negative slopes of the frequency vs. phase shift were present only in the model, and the effect warrants further investigation. The maximum displacement occurred at the same frequency as the midpoint of the change in phase shift. For example, the displacement peak at 155 Hz in the viscous sample with the 8.5 cm cantilever in Fig. 4.5 corresponded to a phase shift of $-35°$, which lies halfway between the plateaus at 65° and $-115°$ at 140 Hz and 170 Hz, respectively. That change in phase shift is about 180°, which is consistent with effects of harmonic resonance. A study on the dependence of phase in resonating systems in

atomic force microscopy found that the phase transforms more quickly at higher resonance modes, which agrees with our results for the changes in phase shift (Fig. 4.5) [144].

Because the trends between the device and the model are similar for the elastic and viscous standards, the device was used to determine the viscoelastic properties of PC tissue.

4.5.3 Viscoelasticity of PC Samples

If the flexural node occurred above the sample where the cantilever's response was recorded, then the tiny amplitudes would be impossible for the laser velocimeter to distinguish from noise. Because the displacement and phase shift data were optimized, it was important to consider only the data that agreed well with its sinusoidal fit. As shown in Fig. 4.6, the waveforms near 330 Hz were not clear sinusoids; the data were also fitted to small amplitudes ($0.05\,\mu$m). Data from PC samples that were eliminated based on poor goodness–of–fit ($R^2 < 0.9$) to the sinusoidal waveform were surrounded by regions of low displacements, which supports the existence of a flexural node at the measured location along the beam.

The resulting sum square errors between the data from representative PC and the system in the simulation, provided in Fig. 4.7, illustrate the sensitivity of the parameters. The displacement–only SSE plot had a band of low error in the Young's modulus centered around ∼150 Pa. This pattern suggests that the Young's modulus is responsible for the height or shape of the frequency vs. displacement curve. Because a wide range of viscosities could produce similar SSE displacements, this data also suggests that the dynamic motion is more dependent on Young's modulus, which does not contain a time–dependent term. Similar effects on frequency dependence of the moduli were shown for soft materials measured by atomic force microscopy [145]. The phase–only SSE contour plot was opposite; it had a band of low error along the viscosity axis with a local minimization around 0.5 Pa·s with a steep increase, especially at low values of Young's modulus. This band suggests that the viscosity term is responsible for a rapid change in phase shift at certain frequencies, or in other words, the viscosity term is more responsible for the location of the peak frequencies.

It is worth noting that displacement and phase shifts were measured on different scales. Although the phase shifts are bound between 0° and 360°, the amplitude of the oscillations are effectively unbounded (none of the largest displacements had poor fits to the sine wave that would indicate nearing the limit of the laser velocimeter). Because the amplitude of the resonance peak is dependent on the viscoelastic parameters, we could not determine a method to normalize the displacement data. The use of two different scales caused difficulties in calculating a combined value of the SSE for optimization. We used a simple multiplier method to weigh the displacement and phase shifts so each would contribute errors of the same order–of–magnitude, yet they remained unequally weighted.

The optimization for the representative PC provided a Young's modulus of 84 Pa and a viscosity of 0.84 Pa·s. At the frequencies tested, both values are on the same order–of–magnitude (0.84 Pa·s × 100 Hz = 84 Pa), suggesting that both elastic and viscous forces are relatively equally responsible for the resulting dynamic mechanics of the tissue at the frequencies of interest. The Young's modulus of 84 Pa for the representative PC was significantly lower than of 1.4 ± 0.86 kPa calculated by Quindlen et al. [64], which is not surprising considering the differences in the methods and the inclusion of dynamic measurements.

In the plots for the resulting displacement and phase shift in Fig. 4.8, it appears that there is better agreement between the device and the model at low frequencies around the location of the first fundamental resonance. A study on the dependence of phase in resonating systems in atomic force microscopy found increased sensitivity to viscosity at higher flexural modes [144], an effect that agrees with our findings from the contour plots that the viscosity has a greater effect on the resonant frequency. Viscosity is highly dependent on temperature. We did not employ any means of controlling or recording the temperature of the samples, and it was possible that the temperature of the sample changed as each experiment progressed. To more accurately capture the temperature effect with the collected data, future optimizations could employ a frequency–dependent temperature term as an estimate as the viscous heating rate. Furthermore, the simplifications discussed below involving treating the sample as a cylinder in the model and not accounting for surface tension between the sample and the cantilever may have served as larger potential sources or error.

4.5.4 Limitations and Future Work

This project attempted to obtain estimates of the viscoelastic parameters of human cadaveric PCs at physiologically–relevant timescales. The cantilever-based device was tested because it allowed the PC to have oscillatory responses in the 100-500 Hz range. Methods like atomic force microscopy (AFM) are commonly limited to 500 Hz minimum driving frequencies [145], and on the other end, the NanoIndentor in the Tissue Mechanics Laboratory is limited to maximum frequencies of about 200 Hz. The size of the tissue was another problem. Tissues of 3 mm diameter are too large for conventional AFMs but too small for indentors. Our system used modular components, such as cantilevers that were available in a variety of thicknesses and could be cut to any size, which enabled us to change the system based on the response of the samples. The use of the laser velocimeter with a dual-input oscilloscope allowed us to simultaneously collect the input and output waveforms, which was required to calculate the phase shift accurately. Although the resulting system was

too complicated to mathematically solve, we were able to create a finite–element model to compare the simulation's outputs with the device's calculated values of displacement and phase shift to optimize the specific viscoelastic components. The method that we developed appeared to solve some major complications unique to PCs while applying methods like optimization that were successfully implemented on other biological projects in the Barocas lab.

The small timescale required very high precision that was difficult to obtain largely from the inability to accurately measure all the physical parts. Firstly, obtaining accurate dimensions of the PC, primarily the height when it was in the system, was difficult because the cantilever was placed on the tissue manually for each sample, and it was inherently imprecise to take a measurement between the piezo and the cantilever. For that reason, the length:height and width:height ratios were determined for about 15 samples and used to calculate the height of the remaining samples. Also, because the beam was manually placed, the force it exerted with no stimuli could differ between samples and between duplicate trials of the same sample. To avoid the repositioning of the cantilever, we attempted to collect the data for the entire frequency sweep as rapidly as possible to prevent the need to disturb the system to rehydrate the sample. We also aimed to avoid excessive PBS around the sample in order to minimize the contribution of the viscosity of water. The hydration of the sample also contributed significant surface tension as evidenced by the large displacement differences due to the inclusion of water between the elastic sample and the beam in Fig. 4.4. Inconsistency in the precise placement ($\pm$1 mm) of the samples contributed unexpectedly significant uncertainty to the amplitude and phase shift data due to variance in the lengths between the sample and the beam ends. The length of the cantilever is one of the most sensitive parameters, and small discrepancies ($\pm$1 mm) had a large impact. Further testing is needed to measure the tolerance of the effect of cantilever length with respect to PC position.

Other complications included gravity because a large beam would naturally bend without any applied stimuli. Great care was needed to properly align the longer cantilevers so both ends were at the same height. Furthermore, the geography of the sample was simplified in the model from an irregular ovoid of the extracted PCs to a perfect cylinder. This simplification would naturally affect the samples with higher aspect ratios. More tests on the sensitivity of the sample size are needed to determine the range of error. In preliminary testing, small alterations ($\pm$1 mm) in sample height and diameter caused a noticeable change in the displacement ($\sim$10%) but negligible changes in the phase or resonant frequencies.

4.6 Preliminary Conclusions

We found that the mean lengths of the PCs from donors (aged 86 and 92) without DD were 2.9 ± 0.2 mm along the long axis and 2.0 ± 0.2 mm for the short axis. The PCs from the donor with DD (93 y.o.) were significantly larger ($p = 0.0132$) than the PCs from the donors without DD. Although there was significant differences between the PCs from the DD donor and those from the non–DD donors, it would be inappropriate to draw conclusions about the role of the disease based only on three donors.

We created a cantilever–based device and a corresponding COMSOL model to determine the viscoelastic properties of extracted human cadaveric PCs and characterized our approach with elastic and viscous samples. We presented preliminary data for a representative extracted human cadaveric PC. For that sample, the Young's modulus was 84 Pa and the viscosity was 0.84 Pa·s. Additional testing to determine tolerances of the physical parameters of the device is recommended before optimizing data from the remaining 106 PCs.

Finally, it is critical to note that this data, even when all the samples have been properly analyzed, represent the viscoelastic properties of a small subset of PCs from three individual donors. Thus, the data do not represent a population distribution, and the data from the subjects may not represent healthy PCs because the donors may have had underlying medical conditions that affected the structure or mechanics of the PCs. We plan on presenting the mean values for Young's modulus and viscosity for each donor similar to the size data in Fig. 4.3, but we must be vigilant in avoiding overstating or over–extrapolating the findings.

4.7 Appendix: Methods for estimating initial conditions

The key factor to consider is that, although the simulations took minutes to run, the error calculation for a given simulation with a new experimental data set could be done nearly instantaneously. By comparing results from a simulation done previously with a new data set, one can quickly determine how well the existing simulation matched the new data, constructing an ordered quintuple (h, R, E, η, e) — that is, if a samples with height h and radius R had modulus E and viscosity η, it could produce simulation results that had a sum of squared error e when compared to the new data set. By making this calculation for every past simulation run, a point cloud in 4-D space can be generated for all previous (h, R, E, *eta*). For the new experiment, the height and radius of the sample are known, hereafter called h_o and R_o.

Once the point cloud has been built for a given set of experiments, the next step is to construct the Delaunay triangulation of the points (*delaunayn* function in MATLAB). The Delaunay triangluation produces a set of pentatopes (4-D simplexes) filling the space. Under the assumption that a function is linear over each pentatope, the minimum value of the function must be a vertex. Because, however, we are concerned only with points in the (h_o, R_o) plane, we seek the minimum within that plane. Therefore, the minimum must occur at the point where one of the trianular faces of one of the pentatopes intersects with the (h_o, R_o) place.

Each pentatope has ten triangular faces (forced by choosing any three of the five pentatope vertices). Because the vertices are defined by points, the triangular surface can be defined by two parameters, s and t, such that

$$\begin{aligned}(h,\, R,\, E,\, \eta) =& (h_1,\, R_1,\, E_1,\, \eta_1) \\ &+ s * (h_2 - h_1,\, R_2 - R_1,\, E_2 - E_1,\, \eta_2 - \eta_1) \\ &+ t * (h_3 - h_1,\, R_3 - R_1,\, E_3 - E_1,\, \eta_3 - \eta_1)\end{aligned} \tag{4.3}$$

where s and t must be positive and (s + t) must be less than or equal to one. Because we seek the intersection of this surface with the (h_o, R_o) plane, equation 4.3 can be solved for s and t as a 2 x 2 linear problem,

$$\begin{bmatrix} h_2 - h_1 & h_3 - h_1 \\ R_2 - R_1 & R_3 - R_1 \end{bmatrix} \begin{bmatrix} s \\ t \end{bmatrix} = \begin{bmatrix} h_o - h_1 \\ R_o - R_1 \end{bmatrix} \tag{4.4}$$

Equation 4.4 can then be used to calculate E and η, and the corresponding linear

interpolation of the error,

$$e = e_1 + s * (e_2 - e_1) + t * (e_3 - e_1) \tag{4.5}$$

can be obtained. Thus, once the Delaunay triangulation has been generated, the algorithm loops through each triangular face of each pentatope, computes its intersection with the (h_o, R_o) place, and checks to confirm that the intersection lies within the triangle (i.e. s and t are within the above–stated bounds). If so, the interpolated error is calculated. If it is smaller than the previous minimum error, it is set as the new minimum. Once the full loop has been calculated, the estimated optimal value is used as an initial guess for fitting the new data set.

Chapter 5

Conclusion and Future Work

5.1 Major Findings

The Pacinian corpuscle presents an interesting structure to investigate as so much remains unknown. The research presented in this dissertation helps to provide more information on how PCs function in healthy skin as well as investigating PCs in patients with Dupuytren disease. The studies used psychophysical studies of how people sense high-frequency vibrations in the PC range with respect to both discrimination and sensitivity and employed computational and experimental characterization of the mechanical behavior of PCs.

In Chapter 2, we demonstrated that the multiphysics model of a single PC contains enough details to recapitulate the trend of the observed discriminability of human subjects. Discriminatbility as predicted by van Rossum distances in the *in silico* experiments correlated well with the discriminability observed in the psychophysical experiments measured by *d'* values. We showed that discriminability of pure sinusoidal vibrational stimuli in the range of PC activation increase as the frequency different between the pairs increase. We found that complex stimuli, i.e. waveforms with two frequency components, were more difficult to discriminate and that neither the psychophysical model nor the model of a PC followed any discernible trend in discrimination of the complex stimuli. Our results suggest that the mulitphysics model is also a behavorial model in that it can recapitulate some of the observed response of the whole organism. The data were published in *IEEE Transactions on Haptics* [52].

In Chapter 3, we continued with psychophysical studies on the ability to sense vibrations and expanded out tests to include subjects with DD in addition to healthy contols. This study was very exciting in its novelty; to the best of our knowledge, no one had previously studied the response to vibrational stimuli in DD patients. We used a Psi-marginal adaptive algorithm to determine vibrotactile perception thresholds in 74 subjects without DD and

36 subjects with DD, and we measured VPT at two locations — fingertip and palm — and two frequencies — 250 and 500 Hz. We formed four main conclusions: i) sensitivity decreases with age, ii) women are more sensitive to frequencies within the PC band, iii) men with DD were less sensitive than men without DD, and iV) the unaffected hand was more sensitive than the affected hand in unilaterally–presenting DD patients. This data presents interesting trends that may serve as a useful reference to future researchers interested in PCs of DD. The data are under review at *The Journal of Plastic Surgery and Hand Surgery* [100], and the full dataset is available online [101].

In Chapter 4, we studied the dynamic viscoelastic properties of the PC with isolated human cadaveric PCs from donors with and without DD at physiologically–relevant timescales. We created a cantilever-based device and an equivalent computational model that stimulated the sample and measured the resulting waveform that passed through the sample and the cantilever. By calculating the displacement at the cantilever above the sample and the phase shift between the cantilever's motion and the input vibrations for both the device and the simulation, we could optimize the parameters for Young's modulus and viscosity. Our preliminary findings on a representative isolated human cadaveric PC had a Young's modulus of 84 Pa and viscosity of 0.84 Pa·s. The mean length of PCs from a donor with DD was significantly larger than the PC length from two donors without DD, which agrees with previous findings. We discussed the complications and recommendations to improve the optimization process for the ongoing analysis.

5.2 Limitations and Future Directions

The majority of the work presented in this thesis used human volunteers or human tissue, both of which have striking limitations. The data from human volunteers are inherently variable, and the physical time and resources that the volunteers are willing to give is often the greatest barrier to overcome. Because this work was not funded, the volunteers donated their time for minimal compensation (in addition to my profound gratitude!), and, consequently, we needed to ensure that the psychophysical experiments could be completed in reasonable amounts of time. Subjects had a wide variety of backgrounds and may have approached the study differently, which only propagated the variabilities and inconsistencies. The cadaveric tissue used in Chapter 4 was a limited resource, and the tissue studied may not accurately represent the general population, especially due to the age of the donors. Nonetheless, we worked to obtain obtain sufficient data to advance the scientific understanding of Pacinian corpuscles and its relationship with Dupuytren disease. This section explains some of the major limitations of each study and suggests aspects upon which our studies can be expanded in the future.

Chapter 2 was limited to a single 30–minute study session, so we selected five frequencies that represented unique features of pairings for both the simple and complex waveforms. It would be interesting to test more frequencies of a greater range. With additional frequencies, especially more base frequencies, trends may appear in pairs with similar or dissimilar compositions, e.g. interference patterns. Additionally, further investigation into frequency discrimination with varying amplitudes and accelerations may provide additional insight into how information is processed by the PC. We used a model of a single PC, whereas expanding the model to include clusters or populations of PCs with different orientations and slightly different sizes and shapes would more accurately predict response to vibrational stimuli. Our model was unable to address population behavior, so we did not study advanced stimuli (e.g. the creation of complex stimuli as two different frequencies from separate initial locations directed the same way).

Limitations for chapter 3 falls into three categories: time constraints, disease variability, and technical complications. Firstly, we collected data at the 2018 Minnesota State Fair, which granted us access to a wide population of people but limited our study to tests that could be completed within a single 10 or 15–minute session. To ensure we tested two locations, we limited the study to two frequencies, which we believed would provide sufficient data to learn more about how the PC functions. After the fair, we were dependent on volunteers willing to travel to the university campus for private tests for minimal compensation, so we expanded the time of the study to 30-60 minutes by testing multiple hands and possibly multiple affected fingers. Expanding this study to more frequencies could provide more detailed information. Secondly, our study contained subjects at many stages of DD progression and who had undergone different treatments. Whereas we did not have a large enough population to test the effects of a specific treatment option on vibrational response, a future study could enroll patients at the time of treatment. Most relevant, however, would be a longitudinal study of if/how the PC's response is altered in subjects with DD and if/how its sensitivity or discriminability is changed after treatment methods; the benefits of a longitudinal study are explained in detail within chapter3. Lastly, we created improved devices (compared to that in chapter 2), yet they contained some very delicate pieces. People are not always very delicate, especially at the State Fair. We faced some technical challenges during data collection which were not discussed in the chapter but which ultimately decreased the number of subjects tested. However, we recognized and learned from the technical challenges and created a more robust device for individual testing after the fair that we could use in future studies.

Chapter 4 shows preliminary work, so naturally, it has the most room for improvement and continued studies. Many details about the future plans to improve and further test the optimization methods are provided in the chapter. Because we only tested PCs from

three donors, all of whom were elderly (86, 92, and 93 years old), it would be useful to test additional PCs from younger patients and from patients with other diseases (e.g. diabetes or connective tissue diseases). Although we tried to obtain PCs from DD patients who were undergoing surgery to remove the Dupuytren cords, there were complications with the specimens, and, unfortunately, we were ultimately unable to test those PCs.

5.3 Significance and Applications

The work presented here contributes to a deeper understanding of the PC, providing novel data on frequency discrimination and vibrational sensitivity and preliminary data on the PC's visceoelastic properties. We investigated whether PCs are altered in DD and provided the first dataset of vibrotactile perception thresholds for patients with DD.

The work can and may be applied to future models of PCs and may be used to better diagnose or prognose Dupuytren disease. Applying the multiphysics model, even with complex stimuli, to haptics applications may be a viable substitute for recruiting volunteers to more rapidly test devices ranging from improved button-click mechanisms for the blind and deaf communities to more stimulating video game controllers. If future studies confirm that men with DD are, indeed, less sensitive to vibrations than healthy controls, then the device that we built for chapter 3 could be expanded as a clinical tool to test or monitor DD patients. Increased knowledge about the fundamental mechanics of PCs can aid in future models, and the device that we created to measure the viscoelastic properties of the PC can be extended to dynamically estimate the viscoelasticity of other soft biological tissues.

Bibliography

[1] Figure 8.4. In *Biological Psychology*. Sinauer Associates, Inc., 7 edition, 2013.

[2] Mariano SH Di Fiore and Victor P Eroschenko. Plate 49, fig. 2. In *Di Fiore's atlas of histology with functional correlations*, page 133. Lea & Febiger, 7 edition, 1993.

[3] Dupuytren's disease: Research update, Oct 2018.

[4] Kenneth O Johnson. The roles and functions of cutaneous mechanoreceptors. *Current opinion in neurobiology*, 11(4):455–461, 2001.

[5] Stanley J Bolanowski Jr, George A Gescheider, Ronald T Verrillo, and Christin M Checkosky. Four channels mediate the mechanical aspects of touch. *The Journal of the Acoustical society of America*, 84(5):1680–1694, 1988.

[6] Amanda Zimmerman, Ling Bai, and David D Ginty. The gentle touch receptors of mammalian skin. *Science*, 346(6212):950–954, 2014.

[7] Jonathan Bell, Stanley Bolanowski, and Mark H Holmes. The structure and function of pacinian corpuscles: a review. *Progress in neurobiology*, 42(1):79–128, 1994.

[8] SJ Bolanowski Jr and Jozef J Zwislocki. Intensity and frequency characteristics of pacinian corpuscles. i. action potentials. *Journal of neurophysiology*, 51(4):793–811, 1984.

[9] Ronald T Verrillo. Vibrotactile sensitivity and the frequency response of the pacinian corpuscle. *Psychonomic Science*, 4(1):135–136, 1966.

[10] Sliman J Bensmaia and Mark Hollins. The vibrations of texture. *Somatosensory & motor research*, 20(1):33–43, 2003.

[11] Emily L Mackevicius, Matthew D Best, Hannes P Saal, and Sliman J Bensmaia. Millisecond precision spike timing shapes tactile perception. *Journal of Neuroscience*, 32(44):15309–15317, 2012.

[12] Franziska KB Freyberger and Berthold Farber. Psychophysics and perceiving granularity. In *2006 14th Symposium on Haptic Interfaces for Virtual Environment and Teleoperator Systems*, pages 387–393. IEEE, 2005.

[13] AJ Brisben, SS Hsiao, and KO Johnson. Detection of vibration transmitted through an object grasped in the hand. *Journal of neurophysiology*, 81(4):1548–1558, 1999.

[14] Yitian Shao, Vincent Hayward, and Yon Visell. Spatial patterns of cutaneous vibration during whole-hand haptic interactions. *Proceedings of the National Academy of Sciences*, 113(15):4188–4193, 2016.

[15] Alison I Weber, Hannes P Saal, Justin D Lieber, Ju-Wen Cheng, Louise R Manfredi, John F Dammann, and Sliman J Bensmaia. Spatial and temporal codes mediate the tactile perception of natural textures. *Proceedings of the National Academy of Sciences*, 110(42):17107–17112, 2013.

[16] Roland S Johansson. Tactile sensibility in the human hand: receptive field characteristics of mechanoreceptive units in the glabrous skin area. *The Journal of physiology*, 281(1):101–125, 1978.

[17] Daniel C Pease and T Andrew Quilliam. Electron microscopy of the pacinian corpuscle. *The Journal of Cell Biology*, 3(3):331–342, 1957.

[18] N Cauna and G Mannan. The structure of human digital pacinian corpuscles (corpuscula lamellosa) and its functional significance. *Journal of anatomy*, 92(Pt 1):1, 1958.

[19] Stanley J. Bolanowski Lorraine Pawson, Norma B. Slepecky. Immunocytochemical identification of proteins within the pacinian corpuscle. *Somatosensory & motor research*, 17(2):159–170, 2000.

[20] Chizuka Ide and Shuichiro Hayashi. Specializations of plasma membranes in pacinian corpuscles: implications for mechano-electric transduction. *Journal of neurocytology*, 16(6):759–773, 1987.

[21] Peter S Spencer and Herbert H Schaumburg. An ultrastructural study of the inner core of the pacinian corpuscle. *Journal of neurocytology*, 2(2):217–235, 1973.

[22] José A Vega, Olivia García-Suárez, Juan A Montaño, Berta Pardo, and Juan M Cobo. The meissner and pacinian sensory corpuscles revisited new data from the last decade. *Microscopy research and technique*, 72(4):299–309, 2009.

[23] TA Quilliam and M Sato. The distribution of myelin on nerve fibres from pacinian corpuscles. *The Journal of physiology*, 129(1):167, 1955.

[24] TR Shanthaveerappa and GH Bourne. New observations on the structure of the pacinian corpuscle and its relation to the perineural epithelium of peripheral nerves. *American Journal of Anatomy*, 112(1):97–109, 1963.

[25] Ferdinando Grandori and Antonio Pedotti. Theoretical analysis of mechano-to-neural transduction in pacinian corpuscle. *IEEE Transactions on Biomedical Engineering*, BME–27(10):559–565, 1980.

[26] Victoria E Abraira and David D Ginty. The sensory neurons of touch. *Neuron*, 79(4):618–639, 2013.

[27] WR Loewenstein and R Skalak. Mechanical transmission in a pacinian corpuscle. an analysis and a theory. *The Journal of physiology*, 182(2):346–378, 1966.

[28] J Vernon Luck. Dupuytren's contracture: a new concept of the pathogenesis correlated with surgical management. *JBJS*, 41(4):635–664, 1959.

[29] MG Hart and G Hooper. Clinical associations of dupuytren's disease. *Postgraduate medical journal*, 81(957):425–428, 2005.

[30] B Cheung, JBF Van Erp, and RW Cholewiak. Anatomical, neurophysiological and perceptual issues of tactile perception. *Tactile displays for orientation, navigation and communication in air, sea and land environments. Neuilly-sur-Sein Cedex (France): NATO Research and Technology Organisation*, pages 1–18, 2008.

[31] Sanne Molenkamp, Roel JM van Straalen, Paul MN Werker, and Dieuwke C Broekstra. Imaging for dupuytren disease: a systematic review of the literature. *BMC musculoskeletal disorders*, 20(1):224, 2019.

[32] Dana Britt DiBenedetti, Dat Nguyen, Laurie Zografos, Ryan Ziemiecki, and Xiaolei Zhou. Prevalence, incidence, and treatments of dupuytren's disease in the united states: results from a population-based study. *Hand*, 6(2):149–158, 2011.

[33] Natasha E Picardo and Wasim S Khan. Advances in the understanding of the aetiology of dupuytren's disease. *the surgeon*, 10(3):151–158, 2012.

[34] PF Early. Population studies in dupuytren's contracture. *The Journal of Bone and Joint Surgery. British volume*, 44(3):602–613, 1962.

[35] George AC Murrell and John T Hueston. Aetiology of dupuytren's contracture. *Australian and New Zealand Journal of Surgery*, 60(4):247–252, 1990.

[36] Rupert F Warren. The pathology of dupuytren's contracture. *British journal of plastic surgery*, 6:224–230, 1953.

[37] Laëtitia Michou, Jean-Luc Lermusiaux, Jean-Pierre Teyssedou, Thomas Bardin, Johann Beaudreuil, and Elisabeth Petit-Teixeira. Genetics of dupuytren's disease. *Joint Bone Spine*, 79(1):7–12, 2012.

[38] Lucy C Lee, Andrew Y Zhang, Alphonsus K Chong, Hung Pham, Michael T Longaker, and James Chang. Expression of a novel gene, mafb, in dupuytren's disease. *The Journal of hand surgery*, 31(2):211–218, 2006.

[39] Shaunak S Desai and Vincent R Hentz. The treatment of dupuytren disease. *The Journal of hand surgery*, 36(5):936–942, 2011.

[40] Guy Foucher, J Medina, and Konstantin Malizos. Percutaneous needle fasciotomy in dupuytren disease. *Techniques in hand & upper extremity surgery*, 5(3):161–164, 2001.

[41] Scott Hadley, Emerson Floyd, John Zhao, and Philip Blazar. Trends in dupuytren treatment in the united states. In *Dupuytren Disease and Related Diseases-The Cutting Edge*, pages 23–27. Springer, 2017.

[42] M Heinrich Seegenschmiedt, Karin Piefel, and Thomas Schneider. Review of radiation therapy for palmar and plantar fibromatosis (dupuytren and ledderhose disease). In *Dupuytren Disease and Related Diseases-The Cutting Edge*, pages 341–355. Springer, 2017.

[43] Sandip Hindocha, John K Stanley, Stewart Watson, and Ardeshir Bayat. Dupuytren's diathesis revisited: evaluation of prognostic indicators for risk of disease recurrence. *The Journal of hand surgery*, 31(10):1626–1634, 2006.

[44] SM Gonzalez and RI Gonzalez. Dupuytren's disease. *Western Journal of Medicine*, 152(4):430, 1990.

[45] N Akyürek, O Ataoğlu, S Cenetoğlu, S Ozmen, T Cavuşoğlu, and R Yavuzer. Pacinian corpuscle hyperplasia coexisting with dupuytren's contracture. *Annals of plastic surgery*, 45(2):220, 2000.

[46] A Von Campe, K Mende, H Omaren, and C Meuli-Simmen. Painful nodules and cords in dupuytren disease. *The Journal of hand surgery*, 37(7):1313–1318, 2012.

[47] Wilfred R Ehrmantant, William P Graham III, Javad Towfighi, Donald R Mackay, and H Paul Ehrlich. A histological and anatomical profile of pacinian corpuscles from dupuytren's contracture and the expression of nerve growth factor receptor. *Plastic and reconstructive surgery*, 114(3):721–727, 2004.

[48] László Józsa, Susanne Demel, Tibor Pintér, Antal Renner, Antal Réffy, Andrea Sántha, and Antal Salamon. Immunopathological study on palmar aponeurosis in dupuytren's disease. *Acta histochemica*, 83(2):153–158, 1988.

[49] Mehmet Oguz Yenidunya, Sibel Yenidunya, and Ergin Seven. Pacinian hypertrophy in a type 2a hand burn contracture and pacinian hypertrophy and hyperplasia in a dupuytren's contracture. *burns*, 35(3):446–450, 2009.

[50] L Józsa, A Salamon, A Réffy, A Renner, S Demel, A Donhöffer, T Pintér, and J Thöring. Fine structural alterations of the palmar aponeurosis in dupuytren's contracture. a combined scanning and transmission electronmicroscopic examination. *Zentralblatt fur allgemeine Pathologie u. pathologische Anatomie*, 134(1):15–25, 1988.

[51] Andrew I Lang-Stevenson. Induction of hyperplasia and hypertrophy of pacinian corpuscles. *British medical journal (Clinical research ed.)*, 288(6422):972, 1984.

[52] Tiffany Louisa Senkow, Nicholas D Theis, Julia C Quindlen-Hotek, and Victor H Barocas. Computational and psychophysical experiments on the pacinian corpuscle's ability to discriminate complex stimuli. *IEEE transactions on haptics*, 12(4):635–644, 2019.

[53] B Stark, T Carlstedt, RG Hallin, and M Risling. Distribution of human pacinian corpuscles in the hand: a cadaver study. *Journal of Hand Surgery*, 23(3):370–372, 1998.

[54] Carl Hopkins, Saul Mate-Cid, Robert Fulford, Gary Seiffert, and Jane Ginsborg. Vibrotactile presentation of musical notes to the glabrous skin for adults with normal hearing or a hearing impairment: thresholds, dynamic range and high-frequency perception. *PloS one*, 11(5), 2016.

[55] Sliman J Bensmaia and Lee E Miller. Restoring sensorimotor function through intracortical interfaces: progress and looming challenges. *Nature Reviews Neuroscience*, 15(5):313–325, 2014.

[56] Benoit P Delhaye, Erik W Schluter, and Sliman J Bensmaia. Robo-psychophysics: Extracting behaviorally relevant features from the output of sensors on a prosthetic finger. *IEEE transactions on haptics*, 9(4):499–507, 2016.

[57] Luke Osborn, Rahul R Kaliki, Alcimar B Soares, and Nitish V Thakor. Neuromimetic event-based detection for closed-loop tactile feedback control of upper limb prostheses. *IEEE transactions on haptics*, 9(2):196–206, 2016.

[58] Julia C Quindlen, Henryk K Stolarski, Matthew D Johnson, and Victor H Barocas. A multiphysics model of the pacinian corpuscle. *Integrative Biology*, 8(11):1111–1125, 2016.

[59] Abhijit Biswas, M Manivannan, and Mandayam A Srinivasan. Multiscale layered biomechanical model of the pacinian corpuscle. *IEEE transactions on haptics*, 8(1):31–42, 2014.

[60] Abhijit Biswas, M Manivannan, and Mandayam A Srinivasan. Vibrotactile sensitivity threshold: Nonlinear stochastic mechanotransduction model of the pacinian corpuscle. *IEEE transactions on haptics*, 8(1):102–113, 2014.

[61] Jonathan Bell and Mark Holmes. Model of the dynamics of receptor potential in a mechanoreceptor. *Mathematical biosciences*, 110(2):139–174, 1992.

[62] Julia C Quindlen, Victor K Lai, and Victor H Barocas. Multiscale mechanical model of the pacinian corpuscle shows depth and anisotropy contribute to the receptor's characteristic response to indentation. *PLoS computational biology*, 11(9), 2015.

[63] Hannes P Saal, Benoit P Delhaye, Brandon C Rayhaun, and Sliman J Bensmaia. Simulating tactile signals from the whole hand with millisecond precision. *Proceedings of the National Academy of Sciences*, 114(28):E5693–E5702, 2017.

[64] Julia C Quindlen, Ellen T Bloom, Laura E Ortega, Amy T Moeller, and Victor H Barocas. Micropipette aspiration of the pacinian corpuscle. *Journal of biomechanics*, 63:104–109, 2017.

[65] SJ Bolanowski Jr and JJ Zwislocki. Intensity and frequency characteristics of pacinian corpuscles. ii. receptor potentials. *Journal of neurophysiology*, 51(4):812–830, 1984.

[66] Kenneth Horch. Coding of vibrotactile stimulus frequency by pacinian corpuscle afferents. *The Journal of the Acoustical Society of America*, 89(6):2827–2836, 1991.

[67] Vernon B Mountcastle, Robert H LaMotte, and Giancarlo Carli. Detection thresholds for stimuli in humans and monkeys: comparison with threshold events in mechanoreceptive afferent nerve fibers innervating the monkey hand. *Journal of Neurophysiology*, 35(1):122–136, 1972.

[68] Vernon B Mountcastle, William H Talbot, Ian Darian-Smith, and Hans H Kornhuber. Neural basis of the sense of flutter-vibration. *Science*, 155(3762):597–600, 1967.

[69] Ove Franzén. The dependence of vibrotactile threshold and magnitude functions on stimulation frequency and signal level: A perceptual and neural comparison. *Scandinavian journal of psychology*, 10(1):289–298, 1969.

[70] Frank A Russo, Paolo Ammirante, and Deborah I Fels. Vibrotactile discrimination of musical timbre. *Journal of Experimental Psychology: Human Perception and Performance*, 38(4):822, 2012.

[71] Yongjae Yoo, Inwook Hwang, and Seungmoon Choi. Consonance of vibrotactile chords. *IEEE transactions on haptics*, 7(1):3–13, 2013.

[72] Sliman J Bensmaıa and Mark Hollins. Complex tactile waveform discrimination. *The Journal of the Acoustical Society of America*, 108(3):1236–1245, 2000.

[73] Mark Hollins and Asgeir Sigurdsson. Vibrotactile amplitude and frequency discrimination in temporomandibular disorders. *Pain*, 75(1):59–67, 1998.

[74] Sliman Bensmaïa, Mark Hollins, and Jeffrey Yau. Vibrotactile intensity and frequency information in the pacinian system: a psychophysical model. *Perception & psychophysics*, 67(5):828–841, 2005.

[75] MCW van Rossum. A novel spike distance. *Neural computation*, 13(4):751–763, 2001.

[76] Martin Rothenberg, Ronald T Verrillo, Stephen A Zahorian, Michael L Brachman, and Stanley J Bolanowski Jr. Vibrotactile frequency for encoding a speech parameter. *The Journal of the Acoustical Society of America*, 62(4):1003–1012, 1977.

[77] Vernon B Mountcastle, William H Talbot, Hideo Sakata, and J Hyvärinen. Cortical neuronal mechanisms in flutter-vibration studied in unanesthetized monkeys. neuronal periodicity and frequency discrimination. *Journal of neurophysiology*, 32(3):452–484, 1969.

[78] Gustavo Deco, Leandro Scarano, and Salvador Soto-Faraco. Weber's law in decision making: integrating behavioral data in humans with a neurophysiological model. *Journal of Neuroscience*, 27(42):11192–11200, 2007.

[79] Genevieve D Goff. Differential discrimination of frequency of cutaneous mechanical vibration. *Journal of experimental psychology*, 74(2p1):294, 1967.

[80] Raymond A. Serway and John W. Jewett. Principles of physics. chapter 14: Superp, pages 487–488. Thomsom Learning, Willard, OH, 3 edition, 2002.

[81] Neil A Macmillan and C. Douglas Creelman. *Detection Theory: A User's Guide*. Press Syndicate of the University of Cambridge, New York, 1991.

[82] Robert D Sorkin. Extension of the theory of signal detectability to matching procedures in psychoacoustics. *The Journal of the Acoustical Society of America*, 34(11):1745–1751, 1962.

[83] Howard L Kaplan, Neil A Macmillan, and C Douglas Creelman. Tables of d-prime for variable-standard discrimination paradigms. *Behavior Research Methods & Instrumentation*, 10(6):796–813, 1978.

[84] Qian Yang and May L Ng. Paired comparison/directional difference test/2-alternative forced choice (2-afc) test, simple difference test/same-different test. In *Discrimination Testing in Sensory Science*, pages 109–134. Elsevier, 2017.

[85] N.T. Carnevale and M.L. Hines. *The NEURON Book*. Cambridge University Press, 2006.

[86] Scinob Kuroki, Junji Watanabe, and Shin'ya Nishida. Dissociation of vibrotactile frequency discrimination performances for supra-threshold and near-threshold vibrations. In *International Conference on Human Haptic Sensing and Touch Enabled Computer Applications*, pages 79–84. Springer, 2012.

[87] Stanley S Stevens. Tactile vibration: Change of exponent with frequency. *Perception & Psychophysics*, 3(3):223–228, 1968.

[88] Jonghyun Ryu, Jaehoon Jung, Gunhyuk Park, and Seungmoon Choi. Psychophysical model for vibrotactile rendering in mobile devices. *Presence: Teleoperators and Virtual Environments*, 19(4):364–387, 2010.

[89] Yuan Wang, MJ Turner, James Perrin, and WT Hewitt. A haptic visualization mapping model—magnitude model of sinusoidal vibration. In *Proc. EuroHaptics Conf.*, 2006.

[90] Ronald T Verrillo. Subjective magnitude functions for vibrotaction. *IEEE Transactions on Man-machine systems*, 11(1):19–24, 1970.

[91] Helena Pongrac. Vibrotactile perception: Differential effects of frequency, amplitude, and acceleration. In *2006 ieee international workshop on haptic audio visual environments and their applications (have 2006)*, pages 54–59. IEEE, 2006.

[92] Helena Pongrac. Vibrotactile perception: examining the coding of vibrations and the just noticeable difference under various conditions. *Multimedia systems*, 13(4):297–307, 2008.

[93] Ewald Gingl, Anna-M Burger, and Friedrich G Barth. Intracellular recording from a spider vibration receptor. *Journal of Comparative Physiology A*, 192(5):551–558, 2006.

[94] ERNST-AUGUST Seyfarth and ANDREW S French. Intracellular characterization of identified sensory cells in a new spider mechanoreceptor preparation. *Journal of neurophysiology*, 71(4):1422–1427, 1994.

[95] DA Henze and G Buzsáki. Action potential threshold of hippocampal pyramidal cells in vivo is increased by recent spiking activity. *Neuroscience*, 105(1):121–130, 2001.

[96] Rogelio Luna, Adrián Hernández, Carlos D Brody, and Ranulfo Romo. Neural codes for perceptual discrimination in primary somatosensory cortex. *Nature neuroscience*, 8(9):1210–1219, 2005.

[97] Adrián Hernández, Antonio Zainos, and Ranulfo Romo. Neuronal correlates of sensory discrimination in the somatosensory cortex. *Proceedings of the National Academy of Sciences*, 97(11):6191–6196, 2000.

[98] Emilio Salinas, Adrian Hernandez, Antonio Zainos, and Ranulfo Romo. Periodicity and firing rate as candidate neural codes for the frequency of vibrotactile stimuli. *Journal of neuroscience*, 20(14):5503–5515, 2000.

[99] Julia C Quindlen-Hotek and Victor H Barocas. A finite-element model of mechanosensation by a pacinian corpuscle cluster in human skin. *Biomechanics and modeling in mechanobiology*, 17(4):1053–1067, 2018.

[100] Tiffany L Senkow, Mahdi Ahmadi, Rajesh Rajamani, Victor H Barocas, and Amy T Moeller. Vibrotactile perception in dupuytren disease. *The Journal of Hand Surgery*, 2020.

[101] Tiffany L Senkow. Vibrotactile perception thresholds. `http://dx.doi.org/10.17632/5j258zrygy.1`, 2020.

[102] Adam C Nunn and Fred B Schreuder. Dupuytren's contracture: emerging insight into a viking disease. *Hand Surgery*, 19(03):481–490, 2014.

[103] Andrew Y Zhang and Jennifer S Kargel. The basic science of dupuytren disease. *Hand clinics*, 34(3):301–305, 2018.

[104] Thomas H Trojian and Stephanie M Chu. Dupuytren's disease: diagnosis and treatment. *American family physician*, 76(1), 2007.

[105] Kristján G Gudmundsson, Reynir Arngrímsson, and Thorbjörn Jónsson. Eighteen years follow-up study of the clinical manifestations and progression of dupuytren's disease. *Scandinavian journal of rheumatology*, 30(1):31–34, 2001.

[106] David B O'Gorman, Linda Vi, and Bing Siang Gan. Molecular mechanisms and treatment strategies for dupuytren's disease. *Therapeutics and clinical risk management*, 6:383, 2010.

[107] G Foucher, C Cornil, E Lenoble, and N Citron. A modified open palm technique for dupuytren's disease. *International orthopaedics*, 19(5):285–288, 1995.

[108] Kate E Elzinga and Michael J Morhart. Needle aponeurotomy for dupuytren disease. *Hand clinics*, 34(3):331–344, 2018.

[109] Lawrence C Hurst, Marie A Badalamente, Vincent R Hentz, Robert N Hotchkiss, F Thomas D Kaplan, Roy A Meals, Theodore M Smith, and John Rodzvilla. Injectable collagenase clostridium histolyticum for dupuytren's contracture. *New England Journal of Medicine*, 361(10):968–979, 2009.

[110] Tony Y Eng, Mustafa Abugideiri, Tiffany W Chen, Nicholas Madden, Tiffany Morgan, Daniel Tanenbaum, Narine Wandrey, Sarah Westergaard, and Karen Xu. Radiation therapy for benign disease: Arteriovenous malformations, desmoid tumor, dupuytren contracture, graves ophthalmopathy, gynecomastia, heterotopic ossification, histiocytosis. *Hematology/Oncology Clinics*, 34(1):205–227, 2020.

[111] Ronald T Verrillo, Stanley J Bolanowski, and George A Gescheider. Effect of aging on the subjective magnitude of vibration. *Somatosensory & motor research*, 19(3):238–244, 2002.

[112] Julia C Quindlen, Burak Güçlü, Eric A Schepis, and Victor H Barocas. Computational parametric analysis of the mechanical response of structurally varying pacinian corpuscles. *Journal of biomechanical engineering*, 139(7):071012, 2017.

[113] Burak Güçlü, Eric A Schepis, Serkan Yelke, Can A Yucesoy, and Stanley J Bolanowski. Ovoid geometry of the pacinian corpuscle is not the determining factor for mechanical excitation. *Somatosensory & motor research*, 23(3-4):119–126, 2006.

[114] Minu Shikha Gandhi, Richard Sesek, Robert Tuckett, and Stacy J Morris Bamberg. Progress in vibrotactile threshold evaluation techniques: a review. *Journal of Hand Therapy*, 24(3):240–256, 2011.

[115] Riccardo Iandolo, Marta Carè, Valay A Shah, Simona Schiavi, Giulia Bommarito, Giacomo Boffa, Psiche Giannoni, Matilde Inglese, Leigh Ann Mrotek, Robert A Scheidt, et al. A two alternative forced choice method for assessing vibrotactile discrimination thresholds in the lower limb. *Somatosensory & motor research*, 36(2):162–170, 2019.

[116] Christian Hatzfeld, Siran Cao, Mario Kupnik, and Roland Werthschützky. Vibrotactile force perception–absolute and differential thresholds and external influences. *IEEE transactions on haptics*, 9(4):586–597, 2016.

[117] Burathat Junput, Xuyi Wei, and Lorenzo Jamone. Feel it on your fingers: Dataglove with vibrotactile feedback for virtual reality and telerobotics. In *Annual Conference Towards Autonomous Robotic Systems*, pages 375–385. Springer, 2019.

[118] Yoshihiro Tanaka, Yuichiro Ueda, and Akihito Sano. Effect of skin-transmitted vibration enhancement on vibrotactile perception. *Experimental brain research*, 233(6):1721–1731, 2015.

[119] Mustafa Zahıd Yildiz and Burak Güçlü. Relationship between vibrotactile detection threshold in the pacinian channel and complex mechanical modulus of the human glabrous skin. *Somatosensory & motor research*, 30(1):37–47, 2013.

[120] David A Mahns, NM Perkins, Vineet Sahai, L Robinson, and MJ Rowe. Vibrotactile frequency discrimination in human hairy skin. *Journal of neurophysiology*, 95(3):1442–1450, 2006.

[121] Miyuki Morioka and Michael J Griffin. Independent responses of pacinian and non-pacinian systems with hand-transmitted vibration detected from masked thresholds. *Somatosensory & motor research*, 22(1-2):69–84, 2005.

[122] David Karpul, Sarah McIntyre, André van Schaik, Paul P Breen, and Jeannine M Heckmann. Vibrotactile sensitivity of patients with hiv-related sensory neuropathy: An exploratory study. *Brain and behavior*, 9(1):e01184, 2019.

[123] Wen Liu, Lewis A Lipsitz, Manuel Montero-Odasso, Jonathan Bean, D Casey Kerrigan, and James J Collins. Noise-enhanced vibrotactile sensitivity in older adults, patients with stroke, and patients with diabetic neuropathy. *Archives of physical medicine and rehabilitation*, 83(2):171–176, 2002.

[124] J Duke, M McEvoy, D Sibbritt, M Guest, W Smith, and J Attia. Vibrotactile threshold measurement for detecting peripheral neuropathy: defining variability and a normal range for clinical and research use. *Diabetologia*, 50(11):2305–2312, 2007.

[125] NOB Thomsen, Ragnhild Cederlund, T Speidel, and LB Dahlin. Vibrotactile sense in patients with diabetes and carpal tunnel syndrome. *Diabetic medicine*, 28(11):1401–1406, 2011.

[126] Nicolaas Prins. The psi-marginal adaptive method: How to give nuisance parameters the attention they deserve (no more, no less). *Journal of vision*, 13(7):3–3, 2013.

[127] Jeremy Stangroom. One-way repeated measures anova calculator, 2020.

[128] Meg Stuart, A Bulent Turman, Jacqueline Shaw, Natalie Walsh, and Vincent Nguyen. Effects of aging on vibration detection thresholds at various body regions. *BMC geriatrics*, 3(1):1, 2003.

[129] Duška Meh and Miro Denišlič. Influence of age, temperature, sex, height and diazepam on vibration perception. *Journal of the neurological sciences*, 134(1-2):136–142, 1995.

[130] Nandini Deshpande, E Jeffery Metter, Shari Ling, Robin Conwit, and Luigi Ferrucci. Physiological correlates of age-related decline in vibrotactile sensitivity. *Neurobiology of aging*, 29(5):765–773, 2008.

[131] Torsten Skov, Kyle Steenland, and James Deddens. Effect of age and height on vibrotactile threshold among 1,663 us workers. *American journal of industrial medicine*, 34(5):438–444, 1998.

[132] P Era, J Jokela, H Suominen, and E Heikkinen. Correlates of vibrotactile thresholds in men of different ages. *Acta neurologica scandinavica*, 74(3):210–217, 1986.

[133] R Lundström, T Strömberg, and G Lundborg. Vibrotactile perception threshold measurements for diagnosis of sensory neuropathy. *International archives of occupational and environmental health*, 64(3):201–207, 1992.

[134] Eva-Maria Reuter, Claudia Voelcker-Rehage, Solveig Vieluf, and Ben Godde. Touch perception throughout working life: Effects of age and expertise. *Experimental Brain Research*, 216(2):287–297, 2012.

[135] Ryan M Peters, Erik Hackeman, and Daniel Goldreich. Diminutive digits discern delicate details: fingertip size and the sex difference in tactile spatial acuity. *Journal of Neuroscience*, 29(50):15756–15761, 2009.

[136] Yoshihiro Tanaka, T Ito, Masayoshi Hashimoto, Motoaki Fukasawa, Nobuteru Usuda, and Akihito Sano. Collagen fibers induce expansion of receptive field of pacinian corpuscles. *Advanced Robotics*, 29(11):735–741, 2015.

[137] SJ Bolanowski Jr and Ronald T Verrillo. Temperature and criterion effects in a somatosensory subsystem: a neurophysiological and psychophysical study. *Journal of Neurophysiology*, 48(3):836–855, 1982.

[138] Chizuka Ide. Role of extracellular matrix in the regeneration of a pacinian corpuscle. *Brain research*, 413(1):155–169, 1987.

[139] TR Shanthaveerappa and GH Bourne. Histochemical studies on the pacinian corpuscle. *American Journal of Anatomy*, 118(2):461–470, 1966.

[140] Kristján G Gudmundsson, Reynir Arngrímsson, Nikulás Sigfússon, Árni Björnsson, and Thorbjörn Jónsson. Epidemiology of dupuytren's disease: clinical, serological, and social assessment. the reykjavik study. *Journal of clinical epidemiology*, 53(3):291–296, 2000.

[141] R_S M Ling. The genetic factor in dupuytren's disease. *The Journal of bone and joint surgery. British volume*, 45(4):709–718, 1963.

[142] Jeffrey C Howard, Vincenzo M Varallo, Douglas C Ross, Kenneth J Faber, James H Roth, Shannon Seney, and Bing Siang Gan. Wound healing-associated proteins hsp47 and fibronectin are elevated in dupuytren's contracture. *Journal of Surgical Research*, 117(2):232–238, 2004.

[143] Sture Holm. A simple sequentially rejective multiple test procedure. *Scandinavian journal of statistics*, pages 65–70, 1979.

[144] Xilong Zhou, Rongshu Zhuo, Pengfei Wen, and Faxin Li. Amplitude modulation atomic force microscopy based on higher flexural modes. *AIP Advances*, 7(12):125319, 2017.

[145] Nan Yang, Kenneth Kar Ho Wong, John R de Bruyn, and Jeffrey L Hutter. Frequency-dependent viscoelasticity measurement by atomic force microscopy. *Measurement Science and Technology*, 20(2):025703, 2008.